

# Deep Learning for Financial Time Series: A Large-Scale Benchmark of Risk-Adjusted Performance\*

Adir Saly-Kaufmann<sup>1</sup>, Kieran Wood<sup>1,2</sup>, Jan Peter-Calliess<sup>1</sup>, Stefan Zohren<sup>1</sup>

<sup>1</sup>Machine Learning Research Group, Department of Engineering Science, University of Oxford

<sup>2</sup>Oxford-Man Institute of Quantitative Finance, University of Oxford

adir.saly-kaufmann@eng.ox.ac.uk, kieran.wood@eng.ox.ac.uk  
janpeter.calliess@eng.ox.ac.uk, stefan.zohren@eng.ox.ac.uk

## Abstract

We present a large-scale benchmark of modern deep learning architectures for a financial time-series prediction and position sizing task, with a primary focus on Sharpe-ratio optimization. Evaluating linear models, recurrent networks, transformer-based architectures, state-space models, and recent sequence-representation approaches, we assess out-of-sample performance on a daily futures dataset spanning commodities, equity indices, bonds, and FX spanning 2010–2025. Our evaluation goes beyond average returns and includes statistical significance, downside and tail-risk measures, breakeven transaction-cost analysis, robustness to random seed selection, and computational efficiency. We find that models explicitly designed to learn rich temporal representations consistently outperform linear benchmarks and generic deep learning models, which often lead the ranking in standard time-series benchmarks. Hybrid models such as VSN + LSTM, a combination of Variable Selection Networks (VSN) and LSTMs, achieves the highest overall Sharpe ratio, while VSN+xLSTM and LSTM+PatchTST exhibit superior downside-adjusted characteristics. xLSTM demonstrates the largest breakeven transaction cost buffer, indicating improved robustness to trading frictions.

\*Code is available upon request.

## 1 Introduction

In recent years, many new deep learning architectures have emerged in the context of time-series forecasting, with Transformer-based architectures [1] drawing particular attention [2]. Several theoretical extensions and adaptations have been proposed, such as iTransformer [3], PatchTST [4], and the Temporal Fusion Transformer [5]. Each of these models aims to address different challenges encountered in real-world forecasting. For example, PatchTST improves robustness by bundling data points and interpreting features independently, whereas iTransformer focuses on learning relationships between features without relying on temporal order.

State Space Models have also presented an alternative to transformer-based architectures. In particular, Mamba2 [6] claims to achieve a mathematically principled architecture with linear-attention-like behavior [7] while supporting arbitrarily large lookback windows. More broadly, State Space Models have evolved from the theory of HiPPO (High-order Polynomial Projection Operators) matrices [8], which maintain compressed representations of past information as the model evolves.

Historically, recurrent neural networks (RNNs) [9] have been the most widely used deep-learning architectures for time-series forecasting [10], especially

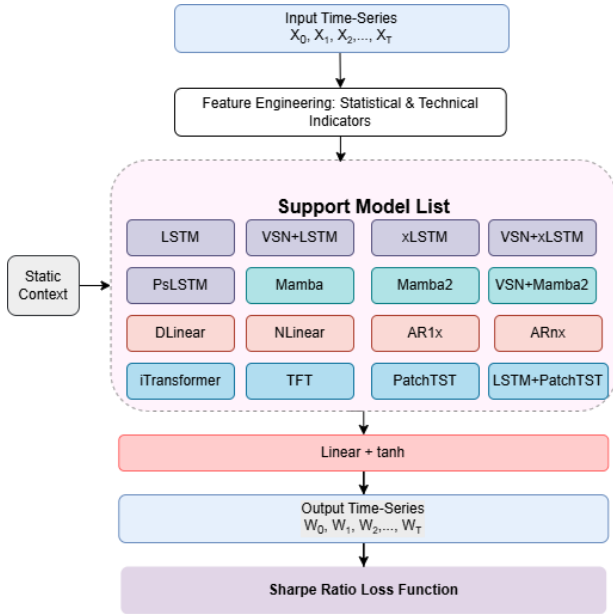


Figure 1: End-to-end portfolio optimization pipeline: Statistical and technical indicators are extracted from historical close prices, serving as the predictive model’s inputs. The model outputs are transformed into portfolio weights via a linear projection followed by a hyperbolic tangent activation. Training is performed by minimizing the negative Sharpe Ratio.

LSTMs [11]. More recently, the xLSTM architecture [12] has been introduced as a new state-of-the-art model, with additional gains demonstrated by PsLSTM [13]. xLSTM replaces LSTM’s traditional sigmoid gating with exponential gating and a normalization term, while also employing a memory matrix rather than a scalar value. PsLSTM further integrates patching (similar to PatchTST) into the xLSTM architecture.

Several benchmark studies have explored deep-learning models for time-series forecasting [14], focusing on applications such as weather prediction, electricity transformer temperatures, and transportation data. These studies indicate that simple architectures such as DLinear [15] can perform comparably to more complex transformer-based models. Similarly, [15] has shown that NLinear performs slightly better in some settings. However, these datasets exhibit

strong seasonality and a high signal-to-noise ratio, in contrast to financial time series [16].

Forecasting financial time series essentially reduces to performing auto-regressive modeling [17], typically formulated as

$$x_{t+1} = f(x_t, x_{t-1}, x_{t-2}, \dots) \quad (1)$$

for each  $0 \leq t < T$ , where  $x_t$  is the value of the process at time  $t$ ,  $T$  is the last time-step to predict, and  $f(\cdot)$  denotes a model-dependent forecasting function that maps past observations to a one-step-ahead prediction. For example, in  $AR(p)$  it is of the form:

$$f(x_t, \dots, x_{t-p}) = \sum_{i=0}^p \phi_i x_{t-i},$$

where  $\{\phi_i\}$  are fixed coefficients [17] and in *LSTM* [11],  $f$  is instead represented by a nonlinear recurrent mapping with learnable gating mechanisms and hidden states B.4.

Financial return series are characterized by strong noise, weak and time-varying predictability, and pronounced non-stationarity. These properties imply that predictive success hinges less on raw model capacity than on the ability to recover economically meaningful signals from highly volatile data. In this context, a successful model must simultaneously (i) improve the signal-to-noise ratio by filtering out transient fluctuations, (ii) learn asset-specific dynamics rather than imposing homogeneous temporal structures, and (iii) embed temporal dependencies in a manner that remains stable across market regimes [18, 19]. Several of the benchmarked architectures incorporate explicit design choices aimed at enhancing one or more of these properties, including feature selection, structured state representations, and temporal aggregation mechanisms [20]. We evaluate both the incremental value of such architectural enhancements and their performance relative to models that natively embed these characteristics, with particular emphasis on robustness across time and economic regimes.

**Contributions.** This paper presented a unified benchmark of modern deep learning architectures

for financial time-series prediction under a Sharpe-ratio optimization framework. Using 15 years of data spanning multiple asset classes and market regimes, we evaluated linear models, recurrent networks, transformer-based architectures, state-space models, and recent sequence-representation approaches across return, risk, robustness, and computational dimensions.

**Linear dynamics alone appear insufficient.** While linear models occasionally performed competitively in specific high-volatility subperiods, they failed to deliver stable performance across time and provided limited incremental value relative to a passive benchmark. This supports the view that financial returns exhibit structural features not fully captured by linear autoregression.

**Architectural inductive bias is decisive.** Non-linear models improved average performance, but outcomes varied substantially across architectures. Generic transformers and state-space models displayed heterogeneous, regime-sensitive behavior. In contrast, VLSTM—designed to learn structured temporal representations—delivered consistently strong and stable risk-adjusted returns, suggesting that representation compression, adaptive memory, and temporal abstraction are particularly valuable in low signal-to-noise environments.

**Robustness and risk control matter as much as returns.** Downside exposure, tail behavior, and stability under reduced seed aggregation materially affected model suitability. VLSTM-based strategies combined competitive returns with moderate drawdowns and remained stable under weaker experimental budgets, indicating that performance was not driven solely by favorable seed selection.

**Asymptotic efficiency does not guarantee empirical superiority.** Although state-space models offer attractive theoretical complexity, empirical effectiveness depended more strongly on inductive bias than on asymptotic scaling alone.

Overall, the results suggest that effective financial forecasting models benefit from jointly denoising returns, learning asset-specific and regime-aware dynamics, and encoding temporal structure in a stable

and adaptive manner. While the conclusions remain conditional on the dataset and backtesting protocol employed, this benchmark provides a transparent reference point for future research in deep learning for finance.

## 2 Architectures

### 2.1 Problem Setup

Let  $\{x_t\}_{t=1}^T$ ,  $x_t \in \mathbb{R}^d$ , denote a multivariate time series of end of day features derived from commodity futures, foreign-exchange (FX) futures, bonds, index, and energy products, including prices, returns, and technical indicators.

Given a fixed lookback window of length  $L$ , the objective is to learn a function

$$f_\theta : \mathbb{R}^{L \times d} \rightarrow [-1, 1], \quad (2)$$

mapping historical observations

$$\mathbf{X}_t = [x_{t-L+1}, \dots, x_t] \quad (3)$$

to a scalar forecast or trading signal used to construct daily positions, where 1 is the upper bound for a full long position and -1 is the lower bound for a full short position.

**Trading Signal Generation** To systematically benchmark different deep learning paradigms, we structure the function  $f_\theta$  as a modular, two-stage pipeline. The first stage consists of a candidate sequence architecture  $g_\phi$  (e.g., LSTM, PatchTST, or Mamba2), which processes the input window to extract a temporal state representation of fixed hidden dimension  $H$ :

$$h_t = g_\phi(\mathbf{X}_t), \quad h_t \in \mathbb{R}^H. \quad (4)$$

The second stage is a unified projection head applied to the terminal hidden state  $h_t$ . This consists of a linear transformation followed by a hyperbolic tangent (tanh) activation function to bound the output:

$$\hat{y}_t = \tanh(w_{\text{lin}}^\top h_t + b_{\text{lin}}), \quad (5)$$

where  $w_{\text{lin}} \in \mathbb{R}^H$  and  $b_{\text{lin}} \in \mathbb{R}$  are learnable weights. All models are trained using rolling windows and evaluated in a fully out-of-sample trading framework. **We added ticker embeddings to all the models** to enhance the learning per individual ticker/asset [21].

**Portfolio Construction** The scalar output  $\hat{y}_{t,k} \in [-1, 1]$  generated by the projection head represents the model’s directional conviction for asset  $k$  at time  $t$ . Because financial assets exhibit vastly different baseline volatilities, we employ a volatility targeting framework to equalize risk contributions across the universe [22–24]. We estimate the ex-ante conditional volatility  $\sigma_{t,k}$  for each asset using an Exponentially Weighted Moving Average (EWMA) estimator (detailed in Appendix A). This estimation induces a time-varying leverage factor, defined as  $\text{vs\_factor}_{t,k} = \frac{1}{\sigma_{t,k}}$ , which dynamically scales position sizes in response to shifting market regimes. Given a constant target portfolio volatility  $\sigma_{\text{tgt}}$  (set to 10% in our empirical evaluation), the realized portfolio weight  $w_{t,k}$  allocated to asset  $k$  is obtained by scaling the neural network’s signal by this leverage factor:

$$w_{t,k} = \hat{y}_{t,k} \left( \frac{\sigma_{\text{tgt}}}{\sigma_{t,k}} \right) = \hat{y}_{t,k} \cdot \sigma_{\text{tgt}} \cdot \text{vs\_factor}_{t,k} \quad (6)$$

Given these target weights, the daily gross strategy return for a specific asset  $k$  realized at time  $t + 1$  is the product of the position taken at the end of day  $t$  and the subsequent asset return  $r_{t+1,k}$ :

$$R_{t+1,k} = w_{t,k} \cdot r_{t+1,k} \quad (7)$$

Assuming an equal risk capital allocation across the  $K$  active assets, the aggregate daily gross portfolio return  $R_{t+1}^{\text{port}}$  is the cross-sectional average of the individual strategy returns:

$$R_{t+1}^{\text{port}} = \frac{1}{K} \sum_{k=1}^K R_{t+1,k} \quad (8)$$

**End-to-end Optimization** Unlike traditional forecasting models that minimize predictive errors,

our framework directly optimizes for risk-adjusted economic performance [24]. To train the parameters  $\theta$  of the network  $f_\theta$ , we compute the Sharpe Ratio over a given training sequence of length  $T$ . Let  $\mathbf{R}^{\text{port}} = \{R_1^{\text{port}}, \dots, R_T^{\text{port}}\}$  represent the sequence of daily portfolio returns. We define the sample estimators for the expected return  $\hat{\mathbb{E}}[R]$  and variance  $\hat{\text{Var}}[R]$  of the portfolio as:

$$\hat{\mathbb{E}}[R] = \frac{1}{T} \sum_{t=1}^T R_t^{\text{port}}, \quad (9a)$$

$$\hat{\text{Var}}[R] = \frac{1}{T} \sum_{t=1}^T \left( R_t^{\text{port}} - \hat{\mathbb{E}}[R] \right)^2. \quad (9b)$$

The loss function  $\mathcal{L}(\theta)$  is defined as the negative differentiable annualized Sharpe Ratio:

$$\mathcal{L}(\theta) = -\widehat{\text{SR}}[R] = -\frac{\hat{\mathbb{E}}[R]}{\sqrt{\hat{\text{Var}}[R] + \epsilon}} \sqrt{252}. \quad (10)$$

where 252 represents the approximate number of trading days in a year, and  $\epsilon$  is a small constant added for numerical stability. By minimizing this loss, the network explicitly learns representations that maximize expected returns while heavily penalizing variance. Following the regime-robust DeepPM framework [25], we compute the Sharpe ratio objective on pooled portfolio returns concatenating all sequences in the batch, following their argument that this is the best proxy for optimising out-of-sample Sharpe ratio. See the end-to-end optimization pipeline in Figure 1.

### Net Returns and Breakeven Transaction Costs

To account for implementation frictions, the net portfolio return  $R_{t+1}^{\text{net}}$  is defined by deducting the costs associated with portfolio turnover:

$$R_{t+1}^{\text{net}} = R_{t+1}^{\text{port}} - \frac{1}{K} \sum_{k=1}^K c_k |w_{t,k} - w_{t-1,k}| \quad (11)$$

where  $c_k$  represents the proportional transaction cost per unit of traded weight for asset  $k$ . Because realistic execution costs vary drastically across the asset universe (e.g., highly liquid short-term interest

rates versus illiquid agricultural commodities), imposing static ex-ante assumptions for  $c_k$  can severely distort cross-sectional performance metrics. Therefore, for model optimization and primary evaluation, we set  $c_k = 0$  for all  $k$  to assess the pure predictive efficacy of the architectures (gross returns). To evaluate resilience to trading frictions without relying on arbitrary assumptions, we conduct a post-hoc, asset-level breakeven transaction cost analysis. For each asset, we compute the breakeven cost  $c_k^*$ , which represents the maximum constant friction that specific asset’s strategy can endure before its cumulative PnL is driven to zero. The formal mathematical definition of  $c_k^*$  and the comprehensive per-asset breakeven results are detailed in Appendix E. As detailed by [25], we ensemble the positions of the top  $S$  seeds based on validation loss to reduce turnover and improve robustness to transactions costs.

## 2.2 Linear Baselines

We include a set of linear models as classical and modern baselines to contextualize the performance of deep architectures. The mathematical background can be found in B.1

**Autoregressive Model (AR1x).** The AR1x model [17] serves as a minimal temporal benchmark, capturing short-term autocorrelation in returns. This model applies AR(1) per feature, since the input has multiple features. Its performance provides a lower bound on the benefit of incorporating temporal context and highlights whether short-horizon dependence alone is sufficient for profitable trading.

**DLinear and NLinear.** DLinear and NLinear [15] are non-recurrent linear models that apply learned linear mappings to fixed-length input windows. DLinear explicitly decomposes the input into trend and seasonal components, while NLinear operates on normalized inputs. These models have shown strong performance on data with pronounced linear structure or seasonality.

## 2.3 Transformer-Based Architectures Without Explicit Recurrence

Within the Transformer B.2 temporal context, i.e., context window, the model learns relative temporal importance. However, it does not explicitly encode a temporal state representation and is therefore susceptible to overfitting to outliers.

Transformer-based models are known to perform well in many tasks, but often struggle with financial time-series forecasting [26, 27]. In the implementation of the following models, we use parallel offset streams so we obtain dense per-timestep outputs, similar to the output of the other models.

**iTransformer.** The inverted Transformer [3] applies attention across feature dimensions rather than time, treating each feature as a token. While this design improves parameter efficiency, it removes explicit temporal recurrence and relies solely on attention to capture dynamics.

**PatchTST.** PatchTST [4] segments the input sequence into temporal patches, which are embedded and processed via self-attention. Representing the data in patches inherently smooths the financial time-series and has shown to improve the performance in long-term forecasting [28]. The receptive field is increased to fully exploit the temporal context captured by the patch-based architecture.

## 2.4 State-Space and Implicitly Recurrent Models

**Mamba and Mamba2.** Mamba models [6, 29] belong to the class of selective state-space models (SSMs) B.3, which maintain a latent state that is updated recursively over time. Unlike attention-based architectures, SSMs provide an implicit temporal recurrence with linear-time complexity, making them well-suited for long sequences and noisy environments such as financial time series.

At a high level, these models update a hidden state, often based on High-order Polynomial Projection Operators (HiPPO) [8], which summarizes past information and produces outputs conditioned on the current

state. The parameters governing the state evolution are dynamically modulated by neural networks conditioned on the input, enabling adaptive temporal dynamics while preserving computational efficiency.

Mamba2 refines this formulation by simplifying the state transition structure and increasing head dimensionality, leading to improved numerical stability and throughput. In our implementation, we use a static HiPPO-based state transition matrix with a fixed horizon, rather than per-step adaptive horizon jitter. This design choice improves noise tolerance [30] and stabilizes learning in the presence of heavy-tailed returns and regime shifts, which are common in financial markets.

## 2.5 Recurrent Models

**LSTM.** Long Short-Term Memory (LSTM) B.4 networks maintain an explicit recurrent state, consisting of a hidden state and a memory cell, that is updated sequentially over time, enabling the model to capture temporal dependencies, but with an exponentially decaying long-horizon temporal state [11]. This architecture has proven to be useful in many cases in finance [18].

**xLSTM.** xLSTM [12] extends the classical LSTM by introducing exponential gating and stabilized memory normalization to improve long-range information retention and gradient flow B.4. While standard LSTMs rely on sigmoid gates that may saturate and induce premature forgetting, xLSTM replaces these with exponentiated gate activations followed by normalization, yielding approximately linear behavior over a wider dynamic range. This modification mitigates vanishing memory effects and allows the model to retain rare but economically meaningful signals.

xLSTM comprises two variants: scalar LSTM (sLSTM), which maintains a scalar memory state updated via normalized exponential gates, and matrix LSTM (mLSTM), which generalizes the memory state to a matrix-valued representation, enabling higher memory capacity and associative recall through key-value storage mechanisms. This design

increases representational richness and improves scalability compared to classical recurrent architectures.

From a financial perspective, the ability to preserve temporally distant but informative signals and adaptively revise memory states is particularly relevant in low signal-to-noise and regime-dependent environments [31].

**Patch sLSTM (PsLSTM).** Patch sLSTM [13] integrates the patching strategy of PatchTST with the recurrent inductive bias of sLSTM. Given a multivariate time series of length  $L$  with  $d$  channels, each channel is treated as an independent univariate sequence and segmented into non-overlapping temporal patches:

$$\tilde{x}_p^{(i)} = \text{Patch} \left( x_{t:t+\ell-1}^{(i)} \right), \quad (i = 1, \dots, d) \quad (12)$$

where  $\ell$  denotes the patch length.

Each patch embedding  $\tilde{x}_p^{(i)}$  is then processed by an sLSTM, with shared parameters across channels:

$$h_p^{(i)} = \text{sLSTM}(h_{p-1}^{(i)}, \tilde{x}_p^{(i)}). \quad (13)$$

This design preserves channel independence while enforcing parameter sharing, preventing premature feature mixing and improving generalization.

By operating at the patch level, PsLSTM reduces sensitivity to high-frequency noise and allows the recurrent mechanism to focus on medium-term temporal structure. The exponential gating of sLSTM further enhances memory persistence across patches, enabling the model to capture regime-level dynamics and rare events. After recurrent processing, hidden states across channels are flattened and projected to form the final prediction.

Patch sLSTM thus combines the noise robustness and efficiency of patch-based modeling with the long-range memory advantages of exponential-gated recurrence, which may be advantageous in financial time series characterized by non-stationary and bad signal-to-noise ratio.

## 2.6 Hybrids

Several hybrid architectures are considered to improve robustness in financial time series by enhanc-

ing the signal-to-noise ratio and stabilizing temporal state updates B.5.

Variable Selection Networks (VSNs) B.5, inspired by the Temporal Fusion Transformer, are used to perform feature-wise nonlinear embedding and dynamic soft selection of relevant covariates at each time step. This mechanism adaptively suppresses noisy or uninformative features.

Another strategy to improve robustness is the inclusion of an LSTM-based temporal encoder prior to the main model. By explicitly maintaining a recurrent state, this preprocessing stage filters high-frequency noise and stabilizes downstream representations.

**VSN+LSTM (VLSTM).** VLSTM combines a VSN with an LSTM encoder to construct a compact temporal state representation. This was the core component of the X-Trend architecture used for constructing sequence representations for few-shot learning in financial time series [32]. The VSN produces dynamically weighted feature embeddings, which are then processed sequentially by an LSTM to aggregate long-range temporal information.

**VSN–Mamba2.** This hybrid augments Mamba2 with a VSN to separate feature selection from temporal modeling. The VSN filters noisy covariates before passing the selected representation to the recurrent state-space model, improving robustness in noisy financial environments.

**LSTM + PatchTST (LPatchTST).** This architecture combines explicit recurrence with attention by using an *LSTM as a channel-wise temporal denoiser* prior to PatchTST. The LSTM stabilizes per-channel representations, while PatchTST aggregates medium- and long-range dependencies across denoised temporal patches.

**VSN + xLSTM (VxLSTM).** In this hybrid, VSN-selected representations are directly fed into an xLSTM. The matrix-valued memory of xLSTM enables the model to capture higher-order temporal in-

teractions and long-range dependencies beyond the capacity of vector-based recurrent architectures.

## 2.7 Complete Structured Model

**Temporal Fusion Transformer (TFT).** TFT [5] integrates gated recurrent layers with interpretable attention mechanisms. A recurrent encoder captures local temporal dynamics, where LSTM is used as the recurrent encoder, while multi-head attention aggregates information across time:

$$\hat{y}_t = \text{Attn}(\text{LSTM}(x_{1:t})). \quad (14)$$

Variable selection networks, static covariate encoders, and gating mechanisms further improve robustness, making TFT a strong benchmark for time-series forecasting and specifically financial forecasting [33].

## 3 Empirical Results

This section presents a comprehensive evaluation of the out-of-sample performance of the considered models across multiple market regimes, performance metrics, and computational dimensions, Appendix D.1. We focus on (i) risk-adjusted returns across subperiods, (ii) aggregate return performance and statistical significance, (iii) downside and tail-risk characteristics, (iv) robustness to seed selection and experimental budget, and (v) the trade-off between predictive performance and computational complexity.

### 3.1 Data Description

Our empirical analysis was conducted on a diversified cross-asset futures and currency dataset [34]. The futures data comprises of instruments from five asset classes: bonds, commodities, energy, foreign exchange, and equity indices. Daily closing prices were used to construct returns and predictive features. For futures, we use continuous contracts formed by linking adjacent maturities using a ratio-adjusted backwards methodology (i.e., back-adjusted to remove roll-induced price jumps). A detailed description of

data construction and exploratory analysis is provided in Appendix A.

The dataset [34] exhibits several well-documented stylized facts of financial time series, including heavy-tailed return distributions, volatility clustering, and strong deviations from Gaussianity. These properties are illustrated formally in Appendix A, where we reported distributional diagnostics (e.g., QQ-plots) and volatility dynamics. As such, the dataset provides a realistic and challenging benchmark for evaluating nonlinear forecasting architectures in a cross-asset setting.

Although the empirical evidence is robust within our cross-asset benchmark, the results should be interpreted as conditional on the specific dataset and period considered. Extending the analysis to alternative markets and sampling frequencies would further clarify the external validity of the findings.

### 3.2 Performance Across Market Regimes

Table 1 reports out-of-sample Sharpe ratios aggregated over multiple overlapping horizons from 2010 to 2024, while Table 11 presents annual Sharpe ratios. Taken together, these results enable an evaluation of year-to-year variability and medium-horizon robustness across distinct market regimes, including the post-GFC recovery, the low-volatility expansion of the mid-2010s, and the elevated-uncertainty environment following 2020.

Several systematic patterns emerge.

First, deep nonlinear sequence models substantially outperform linear benchmarks on most aggregated horizons. While linear specifications such as AR1x, ARnx, DLinear, and NLinear occasionally achieve strong single-year Sharpe ratios—particularly during high-volatility years such as 2020—their performance is highly variable across time. Their long-horizon averages over 2010–2025 remain materially below those of the strongest nonlinear architectures. This instability is consistent with the limited representational flexibility of linear dynamics in environments characterized by non-stationarity, regime shifts, and low signal-to-noise ratios.

In contrast, gated recurrent and hybrid sequence models exhibit both higher average Sharpe ratios and greater intertemporal consistency. The LSTM already delivers strong performance (1.48 over 2010–2025), but its variance across years remains non-negligible. Enhanced recurrent architectures improve further. In particular, VLSTM achieves a 2010–2025 Sharpe ratio of 2.40 and maintains strong performance across subperiods, including 2.25 over 2015–2025 and 1.88 over 2020–2025. Similarly, LPatchTST achieves 2.31 over 2010–2025 and remains stable across all aggregated windows, including 2.34 in the post-2020 regime. The Temporal Fusion Transformer (TFT) also demonstrates robust performance, with 2.27 over 2010–2025 and consistent strength across medium-horizon splits.

These results suggest that architectures combining adaptive gating, representation compression, and structured temporal abstraction are better suited to financial data than either purely linear models or attention-only baselines. The year-by-year breakdown further reveals that top-performing models rarely collapse entirely in adverse years; rather, performance degrades moderately while remaining economically meaningful. This robustness is particularly visible during volatile periods such as 2020–2022.

State-space models such as Mamba and Mamba2 display more heterogeneous behavior. While certain years exhibit strong Sharpe ratios (notably 2020 and 2022 for Mamba2), their aggregated performance remains moderate (0.78 and 0.64 over 2010–2025 for Mamba2 and Mamba, respectively). Augmenting Mamba2 with a Variable Selection Network improves medium-horizon averages (1.10 over 2010–2025), indicating that explicit feature conditioning partially mitigates instability, though it does not close the gap to the strongest recurrent or hybrid models.

Transformer-based patching approaches show mixed results. PatchTST achieves moderate long-run averages (0.76 over 2010–2025), but exhibits higher sensitivity to specific years. In contrast, LPatchTST, which augments patching with stronger sequence modeling, delivers consistently superior and more stable results, suggesting that patch segmentation alone is insufficient without robust temporal state encoding.

Table 1: Out-of-sample Sharpe Ratio by subperiod. Annual Sharpe Ratio in Table 11

Strategy	2010-2025	2015-2025	2010-2015	2015-2020	2020-2025
AR1x	0.77	0.70	0.74	0.06	1.35
AR $nx$	0.63	0.55	0.70	-0.01	1.11
DLinear	0.64	0.64	0.60	0.00	1.28
LSTM	1.48	1.33	1.83	1.60	1.07
VLSTM	<b>2.40</b>	<b>2.25</b>	<b>2.57</b>	<b>2.61</b>	1.88
Mamba2	0.78	0.86	0.54	0.18	1.54
VSN+Mamba2	1.10	1.14	0.95	0.54	1.74
PatchTST	0.76	0.80	0.59	0.57	1.03
LPatchTST	<u>2.31</u>	<u>2.22</u>	2.33	<u>2.11</u>	<b>2.34</b>
PsLSTM	1.74	1.74	1.60	1.84	1.68
TFT	2.27	2.08	<u>2.47</u>	2.08	<u>2.08</u>
VxLSTM	1.69	1.61	1.56	1.48	1.74
xLSTM	1.79	1.84	1.46	1.68	1.99
iTransformer	0.38	0.28	0.60	0.06	0.50
Mamba	0.64	0.28	0.51	-0.01	0.56
NLinear	0.66	0.68	0.60	0.14	1.23

Finally, xLSTM-based architectures demonstrate a compelling balance between performance and stability. The xLSTM achieves a Sharpe ratio of 1.79 over 2010–2025, improving to 1.99 in the 2020–2025 period. VxLSTM yields comparable results (1.69 over 2010–2025), while PsLSTM achieves 1.74. Importantly, these models maintain Sharpe ratios near or above 1.5 across most aggregated horizons, indicating resilience to changing volatility regimes. Their year-level profiles show fewer extreme drawdowns relative to classical LSTM, consistent with the hypothesis that enriched state representations and alternative gating mechanisms enhance adaptability in non-stationary environments.

Taken together, the annual and aggregated results reinforce the central hypothesis of the paper: successful financial forecasting architectures benefit from adaptive memory mechanisms, representation compression, and temporally stable state evo-

lution. Models that incorporate structured gating and persistent state representations dominate both linear baselines and generic state-space formulations across nearly all evaluation horizons. As emphasized throughout, these conclusions remain conditional on the dataset and evaluation framework considered; nevertheless, the consistency across multiple temporal aggregations provides evidence that the observed performance differentials are not driven solely by isolated years or singular market events.

### 3.3 Aggregate Return Performance and Statistical Significance

Table 2 reports full-sample out-of-sample performance under a volatility-targeting constraint of 10%, presenting compound annual growth rates (CAGR) [35], annualized returns (Ann. Ret.), Sharpe Ratio (SR) [36], heteroskedasticity and au-

to correlation consistent  $t$ -statistics ( $t$  HAC) [37], hit rate (Hit) [38], turnover, turnover as a multiple of gross market value (xGMV) [23], and additional diagnostics relative to a passive long-only benchmark: the information ratio (Info. Ratio), HAC  $t$ -statistic relative to passive ( $t$  HAC v Passive), and correlation with passive returns (Corr. v Passive). Collectively, these measures capture economic magnitude, statistical reliability, trading intensity, and incremental value relative to buy-and-hold exposure (see Appendix D), see Appendix D.

VLSTM delivers the strongest overall performance within this framework. It achieves a 23.9% annualized return with a Sharpe ratio of 2.39, exceeding both linear and alternative deep learning benchmarks. Its HAC-adjusted  $t$ -statistic of 8.81 indicates high statistical reliability under heteroskedasticity- and autocorrelation-consistent inference. The hit rate of 58.8% suggests persistent directional accuracy. Relative to the passive benchmark, VLSTM attains an information ratio of 0.854 and an HAC  $t$ -statistic of 3.31, indicating statistically distinguishable excess performance. Its correlation with passive returns (0.404) implies partial independence from broad market exposure and meaningful diversification potential.

The hybrid LPatchTST model achieves comparable economic performance, with a Sharpe ratio of 2.32 and a CAGR of 25.5%. Passive-relative metrics remain elevated (information ratio 0.707;  $t$  HAC 2.75), though modestly below VLSTM. Similarly, the Temporal Fusion Transformer (TFT) delivers strong absolute and relative performance (Sharpe 2.20), reinforcing the importance of structured sequence representations and adaptive gating mechanisms. Across these leading architectures, elevated Sharpe ratios coincide with statistically significant passive-relative improvements, suggesting that gains are not merely attributable to implicit market timing or leverage effects under volatility targeting.

LSTM-based variants, including PsLSTM, VxLSTM, and xLSTM, substantially outperform linear baselines. Notably, xLSTM achieves a Sharpe ratio of 1.80 with a comparatively moderate turnover (482), resulting in one of the strongest passive-relative diagnostics (information ratio 0.798;  $t$  HAC 2.90). This combination of competitive returns and reduced trad-

ing intensity suggests improved efficiency in signal extraction relative to classical LSTM, which requires nearly double the turnover to achieve similar Sharpe ratios. These findings are consistent with the view that enriched state representations can improve the signal-to-trade ratio in noisy financial environments.

Linear benchmarks (AR1x, ARnx, DLinear) exhibit Sharpe ratios below one and comparatively small HAC  $t$ -statistics. Passive-relative metrics are near zero or negative, and correlations with the buy-and-hold benchmark remain moderate. While these models occasionally benefit from favorable return persistence, their aggregate performance indicates limited capacity to extract stable predictive structure under non-stationarity.

State-space models display heterogeneous behavior. Mamba2 reduces trading intensity relative to most deep sequence models (turnover 233) but achieves only moderate economic performance (Sharpe 0.62). Augmenting with a Variable Selection Network improves both Sharpe ratio (0.97) and passive-relative metrics, indicating that explicit feature conditioning enhances stability. Nevertheless, their aggregate performance remains below that of recurrent and hybrid architectures.

The inclusion of iTransformer provides an informative contrast. It exhibits by far the lowest turnover (36) and xGMV (9.2), indicating a highly conservative trading profile with minimal portfolio rebalancing. However, this low implementation intensity coincides with weak economic performance (Sharpe 0.35) and statistically insignificant passive-relative diagnostics. This pattern suggests that extreme turnover reduction may reflect under-reactivity to evolving return signals in non-stationary markets. In the present setting, reduced trading alone does not generate economic value; rather, successful models appear to balance adaptive responsiveness with controlled trading intensity.

Figure 2 visually corroborates these quantitative findings. Leading sequence-based models dominate cumulative PnL trajectories while maintaining relatively smooth performance paths, indicating that elevated Sharpe ratios reflect persistent incremental returns rather than isolated return episodes. As throughout, these findings remain conditional on the

Table 2: 2010–2025 Gross return performance, statistical significance, and passive-relative diagnostics (volatility-targeted at 10%).

Model	CAGR	Ann. Ret.	SR	$t$ (HAC)	Hit	Turnover	xGMV	Info. Ratio	$t$ (HAC) v Passive	Corr. v Passive
Passive	0.0435	0.0476	0.48	1.65	0.531	–	–	–	–	–
AR1x	0.0813	0.0831	0.83	3.12	0.539	353.64	90.421	-0.0086	-0.0305	0.3533
AR $_{nx}$	0.0646	0.0677	0.68	2.52	0.538	280.66	69.525	-0.0829	-0.3011	0.4325
DLinear	0.0750	0.0773	0.77	2.87	0.539	278.41	75.282	0.0141	0.0501	<u>0.2612</u>
LSTM	0.1351	0.1318	1.32	4.56	0.554	948.08	225.769	-0.0637	-0.2303	0.2816
VLSTM	<b>0.2632</b>	<b>0.2388</b>	<b>2.39</b>	<b>8.81</b>	<b>0.588</b>	966.86	218.369	<b>0.8539</b>	<b>3.3071</b>	0.4042
Mamba2	0.0587	0.0620	0.62	2.31	0.546	<u>233.00</u>	<u>58.164</u>	-0.0901	-0.3246	<b>0.2220</b>
VSN+Mamba2	0.0967	0.0973	0.97	3.65	0.555	329.11	78.842	0.1091	0.3936	0.2821
PatchTST	0.0847	0.0864	0.86	3.29	0.541	623.88	198.021	-0.2149	-0.7848	0.5530
LPatchTST	<u>0.2550</u>	<u>0.2323</u>	<u>2.32</u>	<b>8.81</b>	0.577	959.89	211.514	0.7070	2.7470	0.3471
PsLSTM	0.1868	0.1763	1.76	6.83	0.563	823.07	185.496	0.3981	1.5410	0.4862
TFT	0.2398	0.2201	2.20	<u>8.13</u>	<u>0.584</u>	912.81	223.231	0.6665	2.5487	0.3888
VxLSTM	0.1937	0.1821	1.82	6.89	0.574	775.88	159.438	0.4666	1.6727	0.5069
xLSTM	0.1937	0.1796	1.80	6.85	0.568	482.62	91.924	<u>0.7984</u>	<u>2.9042</u>	0.6274
iTransformer	0.0308	0.0353	0.35	1.26	0.529	<b>36.32</b>	<b>9.203</b>	-0.1539	-0.5563	0.4855

dataset and backtesting design considered.

### 3.4 Downside Risk and Tail Behavior

While strong average performance is economically relevant, robustness to adverse market conditions is particularly important in financial applications. Table 3 reported downside and tail-risk metrics, including maximum drawdown (Max DD), Calmar ratio (Calmar), worst three-month Sharpe ratio (Worst 3m Sharpe), minimum annual Sharpe ratio (Min Ann. Sharpe), and 5% conditional value at risk (CVaR 5%).

VLSTM and LPatchTST exhibited comparatively moderate drawdowns alongside relatively high Calmar ratios (1.15 and 1.47, respectively). VLSTM achieved a worst three-month Sharpe ratio of -3.68 and the lowest CVaR among the evaluated models. These results were consistent with comparatively milder tail losses within the sample period.

The smallest maximum drawdown was observed for VxLSTM (-11.8%), accompanied by the highest Calmar ratio (1.64). However, this configuration generated lower average returns relative to VLSTM in the aggregate performance analysis, suggesting a more conservative return profile within the evaluation framework.

In contrast, standard LSTM and PatchTST architectures experienced larger drawdowns and weaker worst-period performance. This pattern indicated

greater sensitivity to extreme market movements during the sample period.

Overall, VLSTM combined comparatively strong average performance with moderate downside risk measures. However, LPatchTST and xLSTM were the most robust and were able to keep a favorable tail behavior. Within the dataset considered, this balance suggested a favorable trade-off between return generation and tail-risk exposure. As throughout, these findings should be interpreted as conditional on the sample period and backtesting design.

### 3.5 Breakeven Transaction Cost

Breakeven transaction cost analysis, Appendix E, reveals substantial cross-asset heterogeneity. The tables report annualised, volatility-rescaled gross and net returns together with annualised turnover and the implied breakeven transaction cost  $c^*$  in basis points.

For VLSTM, several agricultural contracts (e.g., Lumber, Oats elec, and Milk III) exhibit high gross returns but also relatively large breakeven costs (exceeding 20 bps). These contracts are comparatively illiquid therefore they are expected to have high transaction costs and scalability is limited despite their strong gross profitability. A broad middle group demonstrates moderate profitability, with breakeven costs in the range of 5–10 bps. At the lower end, high-turnover contracts (e.g., US 2Y Note Composite Bond and Euro Schatz Bond) display very

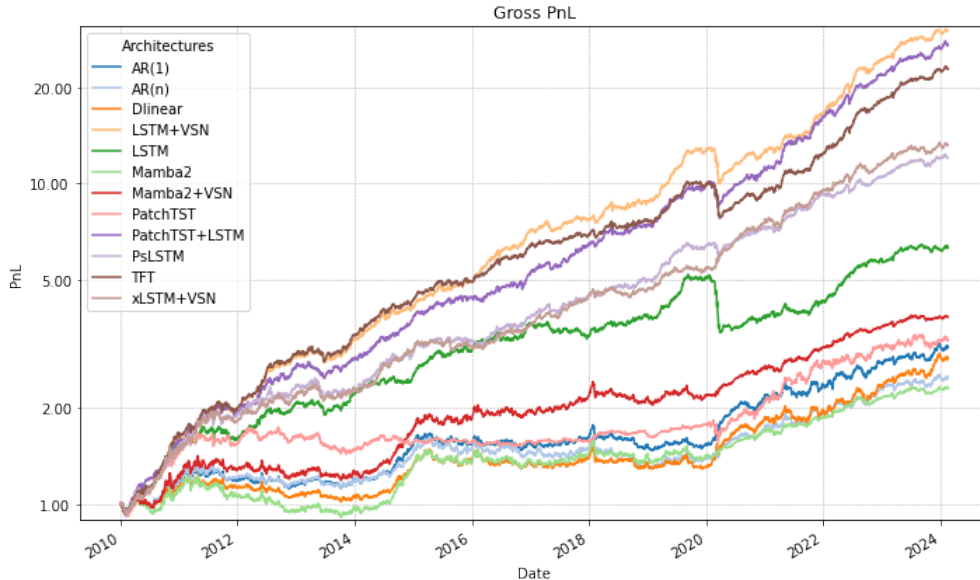


Figure 2: Performance comparison across models 10% volatility-rescaled gross PnL.

small breakeven costs, indicating that profitability is quickly eroded by transaction costs. These are amongst the most liquid contracts; therefore, it is expected that they have tight spreads. However, they can also be traded in high volumes. Finally, a small subset of contracts generates negative gross returns, resulting in negative  $c^*$ .

For xLSTM, the strongest contracts again include Lumber, Oats elec, Milk III, with even higher breakeven costs for some assets (e.g., Lumber at 33.9 bps), once again, noting that these are highly illiquid contracts. Notably, xLSTM achieves materially lower turnover for several equity and bond contracts (e.g., ES, ZN), leading to higher breakeven margins despite similar gross returns. However, the lower tail contains more negative gross performers relative to VLSTM.

Overall, xLSTM appears more transaction-cost efficient in several liquid contracts due to reduced turnover, while VLSTM delivers broader cross-sectional profitability.

### 3.6 Robustness to Seed Selection and Experimental Budget

Table 4 evaluated the robustness of the main findings to a substantially reduced experimental budget. Whereas the primary results in Sections 3.3 and 3.4 were obtained by averaging performance over the top 10 seeds, based on validation loss, from 50 independent runs, this table reported results using only 25 random seeds and averaging over the top 5 realizations. This configuration represented a noisier and more resource-constrained evaluation regime, intended to assess whether model rankings and economic patterns persisted under weaker aggregation.

Across models, performance levels and relative ordering remained broadly stable. VLSTM again achieved the highest absolute and risk-adjusted returns, with a Sharpe ratio of 2.40 and an HAC-adjusted  $t$ -statistic of 8.86, closely aligned with its full-budget estimates. The TFT and VxLSTM also maintained Sharpe ratios above 1.9 with statistically distinguishable HAC  $t$ -statistics, while the linear AR1x benchmark continued to exhibit comparatively weak performance across return metrics. This

Table 3: Downside risk and tail behavior (gross returns).

Model	Max DD	Calmar	Worst 3m Sharpe	Min Ann. Sharpe	CVaR 5%
AR1x	-0.167	0.49	-3.92	-0.59	0.0147
AR $nx$	-0.206	0.31	-4.52	-0.90	0.0148
DLinear	-0.180	0.42	-4.93	-0.94	0.0149
LSTM	-0.342	0.40	-5.15	-1.51	0.0143
VLSTM	-0.229	1.15	<u>-3.68</u>	<u>-0.10</u>	<u>0.0137</u>
Mamba2	-0.263	0.22	-4.06	-0.71	0.0149
VSN+Mamba2	-0.163	0.59	-4.00	-0.63	0.0148
PatchTST	-0.176	0.48	-5.58	-1.21	0.0151
LPatchTST	-0.174	<u>1.47</u>	-3.91	<b>0.51</b>	<b>0.0136</b>
PsLSTM	<u>-0.131</u>	1.43	-3.80	-0.40	0.0143
TFT	-0.232	1.03	-3.87	-0.14	0.0141
VxLSTM	<b>-0.118</b>	<b>1.64</b>	-3.70	-1.31	0.0139
xLSTM	-0.141	1.35	<b>-3.57</b>	-0.28	0.0141
Passive	-0.308	0.14	-6.11	-1.53	0.0144
iTransformer	-0.264	0.12	-3.93	-1.16	0.0154

stability in relative rankings was consistent with the interpretation that performance differences were not solely driven by extensive seed exploration or aggressive averaging.

Downside and tail-risk characteristics exhibited similar patterns. Maximum drawdowns, Calmar ratios, and worst three-month returns remained quantitatively comparable to those observed under the full-budget evaluation. VLSTM and VxLSTM maintained elevated Calmar ratios (1.66 and 1.88, respectively), indicating a similar balance between return generation and drawdown magnitude as in the primary specification. The 5% Conditional Value-at-Risk (CVaR) did not materially deteriorate under reduced seed averaging, suggesting that tail-risk characteristics were not highly sensitive to seed selection within the tested range.

Overall, the reduced-seed experiment suggested that both economic performance and downside risk measures were reasonably stable to substantial reductions in experimental budget. The persistence of model rankings and risk profiles under noisier evaluation conditions was consistent with the view that the

observed performance differences reflected structural properties of the architectures within this benchmark, rather than purely favorable random initialization or extreme-seed selection. As throughout, these conclusions remain conditional on the specific dataset and backtesting protocol employed.

### 3.7 Discussion

The empirical results presented across return, risk, tail, cost, and robustness diagnostics suggest several consistent patterns regarding the inductive biases required for successful financial time-series modeling. As emphasized throughout, these interpretations remain conditional on the dataset and evaluation framework considered, as discussed in Section 3.1.

The dataset exhibits non-stationarity, heavy tails, low signal-to-noise ratios, and pronounced deviations from Gaussianity – stylized facts widely documented in financial return series. To the extent that other financial time series share these characteristics, similar architectural considerations may apply.

Table 4: Reduced-seed benchmark (25 runs, top 5 seeds selected).

Return Performance						Risk and Downside Metrics					
Model	CAGR	Ann. Ret.	Sharpe	$t$ (HAC)	Hit	Model	Max DD	Calmar	Worst 3m	Min Ann.	CVaR 5%
AR1	0.084	0.085	0.854	3.208	0.537	AR1	-0.165	0.506	-4.068	-0.524	0.0147
VLSTM	0.264	0.240	2.397	8.857	0.589	VLSTM	-0.159	1.664	-3.730	-0.250	0.0139
TFT	0.251	0.229	2.290	8.575	0.586	TFT	-0.210	1.196	-3.499	-0.175	0.0141
VxLSTM	0.203	0.190	1.898	7.236	0.578	VxLSTM	-0.108	1.878	-3.718	-1.064	0.0138

First, architectures maintaining explicit recurrent state representations consistently outperformed purely attention-based models across most performance dimensions. This advantage extends beyond average Sharpe ratios to include downside protection and tail behavior. Models such as VLSTM, VxLSTM, and LPatchTST not only achieved strong full-sample Sharpe ratios, but also demonstrated superior Calmar ratios and materially higher minimum annual Sharpe ratios. In particular, LPatchTST exhibited an exceptionally stable worst-year profile, a property of practical relevance in institutional settings where drawdown control and avoidance of severely negative years are often prioritized over marginal improvements in average Sharpe.

Second, robustness must be evaluated multidimensionally. While VLSTM achieved the highest overall Sharpe ratio and strong passive-relative performance, VxLSTM and LPatchTST exhibited superior downside-adjusted characteristics in certain metrics, including Calmar ratio and minimum annual Sharpe. This distinction highlights an economically important trade-off: maximizing mean risk-adjusted return does not necessarily coincide with minimizing drawdown severity or tail exposure. The choice of architecture may therefore depend on investor preference over the mean-tail trade-off.

Third, turnover and transaction cost robustness meaningfully differentiate models. Breakeven transaction cost analysis reveals that xLSTM achieves the highest portfolio-level cost buffer, exceeding VLSTM despite slightly lower average Sharpe. This indicates greater resilience to implementation frictions and a higher signal-to-trade efficiency. Conversely, extremely low-turnover models such as iTransformer exhibit weak predictive performance, suggesting that insufficient responsiveness to evolving signals can be

as detrimental as excessive trading. Successful architectures appear to strike a balance between adaptive state updating and controlled portfolio rebalancing.

Fourth, robustness to seed selection and experimental budget strengthens the credibility of the main findings. Performance rankings remain largely preserved under reduced seed aggregation, indicating that the reported differences are not artifacts of favorable initialization. This stability is particularly important in low signal-to-noise financial environments, where variance across runs can otherwise confound interpretation.

Fifth, state-space models and purely linear benchmarks exhibit heterogeneous and regime-sensitive behavior. While linear models occasionally perform well in high-volatility subperiods, they fail to deliver consistent cross-metric robustness. State-space architectures offer computational efficiency but require additional structure—such as feature selection or enriched state dynamics—to achieve competitive economic performance.

Taken together, the evidence suggests – though does not definitively establish – that successful financial forecasting architectures benefit from: (i) persistent and adaptively gated state representations, (ii) mechanisms for representation compression or feature conditioning, (iii) controlled trading intensity that preserves implementation robustness, and (iv) stability under adverse market realizations. Importantly, the most economically attractive models are not necessarily those with the highest average Sharpe, but those that jointly balance return, drawdown control, tail resilience, and transaction cost tolerance within realistic deployment constraints.

### 3.8 Computational Efficiency and Model Complexity

Table 5 reported parameter counts as well as asymptotic runtime and memory complexities across models. The final number of trainable parameters and the corresponding hyperparameter ranges are provided in Appendix C. Linear models exhibited minimal computational costs in terms of both parameterization and asymptotic complexity, although their empirical performance in previous subsections was comparatively weaker within this benchmark.

Among nonlinear architectures, VLSTM combined competitive empirical performance with linear memory complexity in sequence length and without quadratic attention terms. Relative to transformer-based models such as PatchTST or TFT, this resulted in lower asymptotic memory growth with respect to sequence length. Mamba and Mamba2 offered comparable asymptotic efficiency, though their empirical performance in this study was more heterogeneous across evaluation metrics.

Hybrid architectures, including LPatchTST and VSN-enhanced variants, involved higher parameter counts and additional computational overhead. Within the present evaluation, these increases in complexity were not uniformly associated with proportional performance improvements. This pattern suggested that asymptotic complexity alone did not determine empirical effectiveness, and that architectural inductive bias may play an important role in financial time-series modeling. As with all preceding results, these observations are conditional on the specific dataset, sequence lengths, and implementation choices considered.

## 4 Conclusions

This paper presented a comprehensive benchmark of deep learning architectures for financial time-series prediction under a unified experimental framework spanning 15 years, multiple asset classes, heterogeneous market regimes, and a broad set of economic and statistical diagnostics. Models were evaluated not only on average risk-adjusted returns, but also

on downside risk, tail exposure, transaction cost robustness, implementation intensity, and sensitivity to random initialization.

Several robust patterns emerged:

**First**, purely linear models exhibited occasional regime-specific competitiveness but failed to deliver stable multi-metric performance. Their limited adaptability to non-stationarity and structural change constrained their long-horizon effectiveness.

**Second**, architectures explicitly designed to learn structured and adaptively gated temporal representations consistently outperformed generic attention-based and state-space alternatives. VLSTM achieved the highest overall Sharpe ratio and strong passive-relative performance. However, models such as VxLSTM and LPatchTST demonstrated superior downside-adjusted robustness, including stronger Calmar ratios and more stable worst-year outcomes. These results highlight that mean risk-adjusted return and drawdown resilience need not coincide, and that investor objectives may favor different architectural trade-offs.

**Third**, transaction cost robustness meaningfully differentiates models. xLSTM achieved the highest breakeven cost buffer at the portfolio level, indicating improved signal-to-trade efficiency. Extremely low-turnover architectures, such as iTransformer, exhibited limited predictive strength, suggesting that insufficient responsiveness to evolving signals may undermine economic performance. Effective models appear to balance adaptive state updating with disciplined trading intensity.

**Fourth**, performance rankings remained largely stable under reduced seed aggregation and experimental budgets, reinforcing that observed differences are not artifacts of favorable initialization or excessive tuning.

**Collectively**, the evidence suggests that successful financial forecasting architectures benefit from persistent and adaptively gated state representations, representation compression or feature conditioning mechanisms, and efficient translation of predictive signals into implementable portfolio decisions. Importantly, the most economically attractive models are those that jointly balance average return, drawdown control, tail robustness, and implementation

Model	Number of Parameters	Runtime Complexity	Memory Complexity
TFT	$O(CH^2 + \ell H^2)$	$O(L^2H + LCH^2)$	$O(L^2 + LH)$
VLSTM	$O(CH^2 + H^2)$	$O(LCH^2 + LH^2)$	$O(LH)$
Mamba	$O(\ell H^2)$	$O(LH^2)$	$O(LH)$
Mamba2	$O(\ell H^2)$	$O(LH^2)$	$O(LH)$
VSN + Mamba2	$O(CH^2 + \ell H^2)$	$O(LCH^2 + LH^2)$	$O(LH)$
AR1x	$\mathbf{O(1)}$	$\mathbf{O(L)}$	$\mathbf{O(1)}$
LSTM	$O(H^2 + CH)$	$O(LH^2)$	$O(LH)$
NLinear	$\frac{O(LC)}{O(LC)}$	$\frac{O(LC)}{O(LC)}$	$\frac{O(LC)}{O(LC)}$
DLinear	$\frac{O(LC)}{O(LC)}$	$\frac{O(LC)}{O(LC)}$	$\frac{O(LC)}{O(LC)}$
xLSTM	$\frac{O(H^2 + CH)}{O(LH^2)}$	$\frac{O(LH^2)}{O(LH^2)}$	$\frac{O(LH)}{O(LH)}$
Patch sLSTM	$O(PCH + H^2)$	$O(NH^2)$	$O(NH)$
VSN + xLSTM	$O(H^2(C + H))$	$O(LH^2)$	$O(LH^2)$
PatchTST	$O(PCH + \ell H^2)$	$O(N^2H)$	$O(N^2 + NH)$
LSTM + PatchTST	$O(H^2 + PCH + \ell H^2)$	$O(LH^2 + N^2H)$	$O(LH + N^2)$
iTransformer	$O(\ell H^2)$	$O(C^2H + LCH)$	$O(C^2 + LC)$

Table 5: Comparison of parameter count, runtime complexity, and memory complexity for different time-series forecasting models. The emphasis on order of results is as follows: **best**, second\_best, *third\_best*. The forecasting horizon is fixed to one.  $L$ =sequence length,  $C$ =number of input features,  $H$ =hidden dimension,  $N=L - S$ =number of patches (for shifted versions adjusted for each time step),  $P$ =patch length,  $S$ =stride,  $K$ =convolution kernel size,  $\ell$ =number of layers,  $M$ =number of attention heads.

feasibility.

The conclusions remain conditional on the dataset, market universe, and backtesting assumptions employed. Nevertheless, by evaluating models under realistic non-stationarity, heavy tails, volatility clustering, and transaction cost constraints, this benchmark aims to reflect the statistical and economic challenges inherent to practical financial forecasting. We hope it provides a transparent empirical reference point for future research and encourages architectural development guided not only by computational considerations, but also by the distinctive structural properties of financial markets.

## Acknowledgments

Kieran Wood would like to thank the Oxford-Man Institute of Quantitative Finance for its generous support.

## References

- [1] Ashish Vaswani, Noam Shazeer, Niki Parmar, Jakob Uszkoreit, Llion Jones, Aidan N. Gomez, Łukasz Kaiser, and Illia Polosukhin. Attention is all you need. In Advances in Neural Information Processing Systems, volume 30, 2017.
- [2] Saidul Islam, Hanae Elmekki, Ahmed Elsebai, Jamal Bentahar, Najat Drawel, Gaith Rjoub, and Witold Pedrycz. A comprehensive survey on applications of transformers for deep learning tasks. Expert Systems with Applications, 241: 122666, 2024. doi: 10.1016/j.eswa.2023.122666.
- [3] Yong Liu, Tengge Hu, Haoran Zhang, Haixu Wu, Shiyu Wang, Lintao Ma, and Mingsheng Long. iTransformer: Inverted transformers are effective for time series forecasting. In International Conference on Learning Representations (ICLR), 2024. doi: 10.48550/arXiv.2310.06625. URL <https://openreview.net/forum?id=JePfAI8fah>.
- [4] Yuqi Nie, Nam H. Nguyen, Phanwadee Sinthong,

- and Jayant Kalagnanam. A time series is worth 64 words: Long-term forecasting with transformers. In International Conference on Learning Representations (ICLR), 2023. doi: 10.48550/arXiv.2211.14730. URL <https://openreview.net/forum?id=Jbdc0vT0col>.
- [5] Bryan Lim, Sercan Ö. Arik, Nicolas Loeff, and Tomas Pfister. Temporal fusion transformers for interpretable multi-horizon time series forecasting. International Journal of Forecasting, 37(4):1748–1764, 2021. doi: 10.1016/j.ijforecast.2021.03.012. URL <https://doi.org/10.1016/j.ijforecast.2021.03.012>.
- [6] Tri Dao and Albert Gu. Transformers are SSMs: Generalized models and efficient algorithms through structured state space duality, 2024. URL <https://arxiv.org/abs/2405.21060>.
- [7] Angelos Katharopoulos, Apoorv Vyas, Nikolaos Pappas, and François Fleuret. Transformers are RNNs: Fast autoregressive transformers with linear attention. In Proceedings of the 37th International Conference on Machine Learning (ICML), volume 119 of Proceedings of Machine Learning Research, 2020. doi: 10.48550/arXiv.2006.16236. URL <https://arxiv.org/abs/2006.16236>.
- [8] Albert Gu, Tri Dao, Stefano Ermon, Atri Rudra, and Christopher Ré. HiPPO: Recurrent memory with optimal polynomial projections. In Advances in Neural Information Processing Systems, volume 33, pages 1474–1487, 2020. URL <https://arxiv.org/abs/2008.07669>.
- [9] Leo Feng, Felix Tung, Mostofa O. Ahmed, Yoshua Bengio, and Houd Hajimirsadeghi. Were RNNs all we needed?, 2024. URL <https://arxiv.org/abs/2410.01201>.
- [10] Hansika Hewamalage, Christoph Bergmeir, and Kasun Bandara. Recurrent neural networks for time series forecasting: Current status and future directions. International Journal of Forecasting, 37(1):388–427, 2021. doi: 10.1016/j.ijforecast.2020.06.008. URL <https://arxiv.org/abs/1909.00590>.
- [11] Sepp Hochreiter and Jürgen Schmidhuber. Long short-term memory. Neural Computation, 9(8):1735–1780, 1997. doi: 10.1162/neco.1997.9.8.1735.
- [12] Maximilian Beck, Konstantin Pöppel, Markus Spanring, Andreas Auer, Olga Prudnikova, Michael Kopp, Günter Klambauer, Johannes Brandstetter, and Sepp Hochreiter. xLSTM: Extended long short-term memory. In Advances in Neural Information Processing Systems, volume 37, 2024. doi: 10.48550/arXiv.2405.04517. URL <https://arxiv.org/abs/2405.04517>.
- [13] Yaxuan Kong, Zepu Wang, Yuqi Nie, Tian Zhou, Stefan Zohren, Yuxuan Liang, Peng Sun, and Qingsong Wen. Unlocking the power of LSTM for long term time series forecasting. In Proceedings of the AAAI Conference on Artificial Intelligence, volume 39, pages 11968–11976, 2025. doi: 10.1609/aaai.v39i11.33303. URL <https://ojs.aaai.org/index.php/AAAI/article/view/33303>.
- [14] Yuxuan Wang, Haixu Wu, Jiaxiang Dong, Yong Liu, Chen Wang, Mingsheng Long, and Jianmin Wang. Deep time series models: A comprehensive survey and benchmark, 2024. URL <https://arxiv.org/abs/2407.13278>.
- [15] Ailing Zeng, Muxi Chen, Lei Zhang, and Qiang Xu. Are transformers effective for time series forecasting? In Proceedings of the AAAI Conference on Artificial Intelligence, volume 37, pages 11121–11128, 2023. doi: 10.1609/aaai.v37i9.26317. URL <https://ojs.aaai.org/index.php/AAAI/article/view/26317>.
- [16] Rama Cont. Empirical properties of asset returns: Stylized facts and statistical issues. Quantitative Finance, 1(2):223–236, 2001. doi: 10.1080/713665670.
- [17] George Udny Yule. On a method of investigating periodicities in disturbed series, with

- special reference to wolfer’s sunspot numbers. *Philosophical Transactions of the Royal Society of London. Series A*, 226:267–298, 1927. doi: 10.1098/rsta.1927.0007. URL <https://www.jstor.org/stable/91170>.
- [18] Omer Berat Sezer, Mehmet Ugur Gudelek, and Ahmet Mert Ozbayoglu. Financial time series forecasting with deep learning: A systematic literature review: 2005–2019, 2019. URL <https://arxiv.org/abs/1911.13288>.
- [19] Xinhe Liu and Wenmin Wang. Deep time series forecasting models: A comprehensive survey. *Mathematics*, 12(10):1504, 2024. doi: 10.3390/math12101504. URL <https://www.mdpi.com/2227-7390/12/10/1504>.
- [20] Mateusz Buczyński, Marcin Chlebus, Katarzyna Kopczewska, and Marcin Zajenkowski. Financial time series models—comprehensive review of deep learning approaches and practical recommendations. *Engineering Proceedings*, 39(1):79, 2023. doi: 10.3390/engproc2023039079. URL <https://www.mdpi.com/2673-4591/39/1/79>.
- [21] Cheng Guo and Felix Berkhahn. Entity embeddings of categorical variables. *arXiv preprint arXiv:1604.06737*, 2016. URL <https://arxiv.org/abs/1604.06737>.
- [22] Tobias J. Moskowitz, Yao Hua Ooi, and Lasse Heje Pedersen. Time series momentum. *Journal of Financial Economics*, 104(2): 228–250, 2012. doi: 10.1016/j.jfineco.2011.11.003. URL <https://www.sciencedirect.com/science/article/pii/S0304405X11002613>.
- [23] Campbell R. Harvey, Edward Hoyle, Rohit Kogeaonkar, Sandy Rattray, Matthew Sargaison, and Otto Van Hemert. The impact of volatility targeting. *The Journal of Portfolio Management*, 45(1):14–33, 2018. doi: 10.3905/jpm.2018.45.1.014.
- [24] Bryan Lim, Stefan Zohren, and Stephen Roberts. Enhancing time-series momentum strategies using deep neural networks. *The Journal of Financial Data Science*, 1(4):19–38, 2019. doi: 10.3905/jfds.2019.1.015.
- [25] Kieran Wood, Stephen J. Roberts, and Stefan Zohren. DeePM: Regime-robust deep learning for systematic macro portfolio management, 2026. URL <https://arxiv.org/abs/2601.05975>.
- [26] Yufa Zhou, Yixiao Wang, Surbhi Goel, and Anru R. Zhang. Why do transformers fail to forecast time series in-context?, 2025. URL <https://arxiv.org/abs/2510.09776>.
- [27] Yong Liu, Haixu Wu, Jianmin Wang, and Mingsheng Long. Non-stationary transformers: Exploring the stationarity in time series forecasting, 2022. URL <https://arxiv.org/abs/2205.14415>.
- [28] José M. Oliveira and Pedro Ramos. Evaluating the effectiveness of time series transformers for demand forecasting. *Mathematics*, 12(17):2728, 2024. doi: 10.3390/math12172728. URL <https://www.mdpi.com/2227-7390/12/17/2728>.
- [29] Albert Gu and Tri Dao. Mamba: Linear-time sequence modeling with selective state spaces. In *Proceedings of the First Conference on Language Modeling (COLM)*, 2024. doi: 10.48550/arXiv.2312.00752. URL <https://openreview.net/forum?id=tEYskw1VY2>.
- [30] Albert Gu, Karan Goel, and Christopher Ré. Efficiently modeling long sequences with structured state spaces. In *International Conference on Learning Representations (ICLR)*, 2022. doi: 10.48550/arXiv.2111.00396. URL <https://openreview.net/forum?id=uYLFoz1v1AC>.
- [31] Carl Fjellström. Long short-term memory neural network for financial time series, 2022. URL <https://arxiv.org/abs/2201.08218>.
- [32] Kieran Wood, Samuel Kessler, Stephen J. Roberts, and Stefan Zohren. Few-shot learning patterns in financial time series for trend-following strategies. *The Journal of Financial*

- Data Science, 6(2):88–115, 2024. doi: 10.3905/jfds.2024.1.157.
- [33] Kieran Wood, Sven Giegerich, Stephen Roberts, and Stefan Zohren. Trading with the momentum transformer: An intelligent and interpretable architecture, 2021. URL <https://arxiv.org/abs/2112.08534>.
- [34] Pinnacle Data Corp. Pinnacle data corp. CLC database. Website. URL <https://pinnacledata2.com/clc.html>.
- [35] Edwin J. Elton, Martin J. Gruber, Stephen J. Brown, and William N. Goetzmann. Modern Portfolio Theory and Investment Analysis. John Wiley & Sons, 9 edition, 2014.
- [36] William F. Sharpe. The sharpe ratio. Journal of Portfolio Management, 21(1):49–58, 1994.
- [37] Whitney K. Newey and Kenneth D. West. A simple, positive semi-definite, heteroskedasticity and autocorrelation consistent covariance matrix. Econometrica, 55(3):703–708, 1987.
- [38] M. Hashem Pesaran and Allan Timmermann. A simple nonparametric test of predictive performance. Journal of Business & Economic Statistics, 10(4):461–465, 1992.
- [39] Cheng Zhang, Nilam Nur Amir Sjarif, and Roslina Ibrahim. Deep learning models for price forecasting of financial time series: A review of recent advancements (2020–2022), 2023. URL <https://arxiv.org/abs/2304.11228>.
- [40] Andrea Bucci. Realized volatility forecasting with neural networks. Journal of Financial Econometrics, 18(3):502–531, 2020. doi: 10.1093/jjfinc/nbaa008. URL <https://academic.oup.com/jfec/article/18/3/502/5856840>.
- [41] Teuvo Kohonen. Correlation matrix memories. IEEE Transactions on Computers, C-21(4):353–359, 1972. doi: 10.1109/TC.1972.5008975.
- [42] James A. Anderson. A simple neural network generating an interactive memory. Mathematical Biosciences, 14:197–220, 1972. doi: 10.1016/0025-5564(72)90075-2.
- [43] K. Nakano. Associatron—a model of associative memory. IEEE Transactions on Systems, Man, and Cybernetics, SMC-2(3):380–388, 1972. doi: 10.1109/TSMC.1972.4309133.
- [44] John R. Anderson, James W. Silverstein, Steven A. Ritz, and Randall S. Jones. Distinctive features, categorical perception, and probability learning: Some applications of a neural model. Psychological Review, 84(5):413–451, 1977. doi: 10.1037/0033-295X.84.5.413.
- [45] Diederik P. Kingma and Jimmy Ba. Adam: A method for stochastic optimization. In International Conference on Learning Representations, 2015.

## A Data Construction and Exploratory Analysis

This appendix documents the construction of all variables used in the empirical analysis and provides detailed evidence on their distributional properties.

### A.1 Raw Data and Return Construction

The raw dataset consists of daily observations with three fields: date, ticker, and closing price. From these, daily returns are computed as

$$r_t = \frac{P_t - P_{t-1}}{P_{t-1}}, \quad (15)$$

where  $P_t$  denotes the closing price at time  $t$ .

### A.2 Volatility Estimation

Daily volatility is estimated using an exponentially weighted moving average (EWMA) estimator. Let  $\lambda = \frac{2}{\text{span}+1}$ . The conditional mean and variance evolve according to

$$\mu_t = \lambda r_t + (1 - \lambda)\mu_{t-1}, \quad (16)$$

$$\sigma_t^2 = \lambda(r_t - \mu_t)^2 + (1 - \lambda)\sigma_{t-1}^2. \quad (17)$$

### A.3 Distribution of Returns and Volatility

Figure 3 reports the empirical distribution of daily returns across all assets. The distribution is sharply peaked around zero and exhibits pronounced leptokurtosis. Figure 4 shows the distribution of realized volatility on a logarithmic scale, highlighting strong right skewness and a long upper tail.

Figure 5 presents a quantile–quantile plot against the normal distribution together with the tail behavior of absolute returns. Both figures indicate substantial deviations from Gaussianity and slow tail decay.

### A.4 Predictive Features

Normalized returns are constructed over multiple horizons (1 day, 1 week, 1 month, 3 months, 6

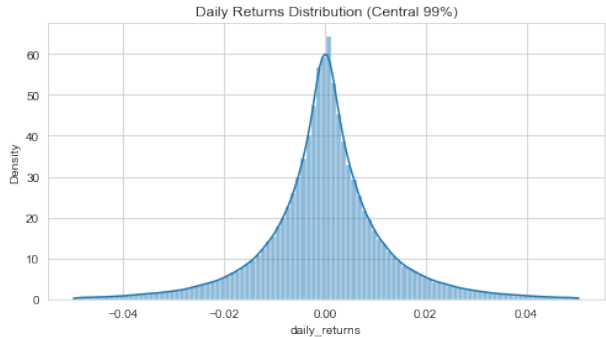


Figure 3: Distribution of daily returns. To make the central mass visible, the figure focuses on the bulk of the distribution; tail behavior is examined separately.

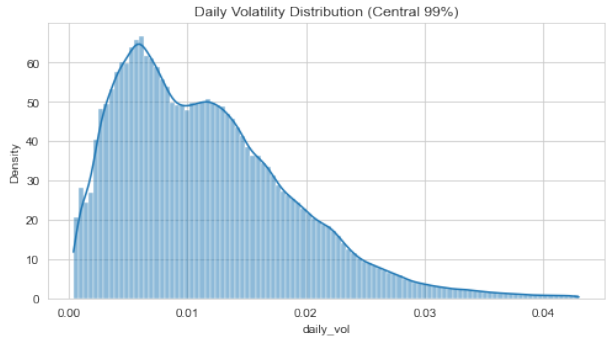


Figure 4: Distribution of daily realized volatility (log scale). Volatility exhibits strong right skewness and a long upper tail.

months, and 1 year) as

$$r_{t,h}^{\text{norm}} = \frac{r_{t,h}}{\sigma_t \sqrt{h}}, \quad (18)$$

where  $h$  denotes the horizon in trading days.

Momentum indicators are further augmented using volatility-normalized and regime-adjusted *Moving Average Convergence Divergence* (MACD) sig-

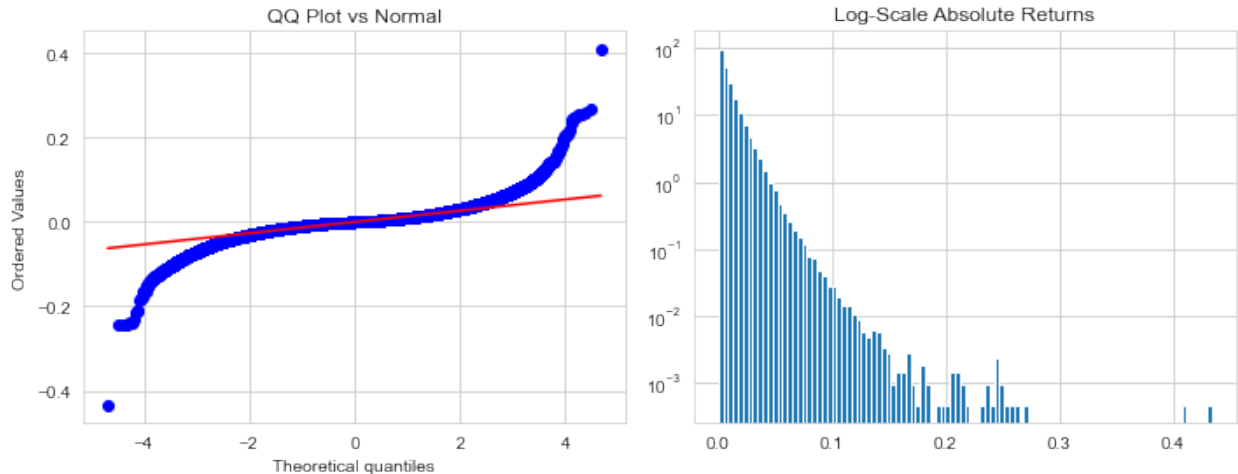


Figure 5: Left: Quantile–quantile plot against the normal distribution. Right: Tail behavior of daily returns. The figures indicate substantial deviations from Gaussianity and heavy-tailed return dynamics.

nals:

$$\text{MACD}_t = \text{EWMA}_{h(T_s)}(P)_t - \text{EWMA}_{h(T_l)}(P)_t, \quad (19)$$

$$q_t = \frac{\text{MACD}_t}{\text{Std}_{63}(P)_t}, \quad (20)$$

$$\text{Signal}_t = \frac{q_t}{\text{Std}_{252}(q)_t}. \quad (21)$$

The empirical distributions of these features are approximately symmetric and concentrated within the interval  $[-2, 2]$ , with nearly all observations contained in  $[-4, 4]$ , as shown in Figure 6.

## A.5 Volatility-Scaled Exposure and Target Variable

Volatility targeting induces a time-varying exposure factor defined as

$$\text{vs\_factor}_t = \frac{1}{\sigma_t}. \quad (22)$$

The empirical distribution of  $\text{vs\_factor}$  exhibits pronounced right skewness, Figure 7. A large share of the mass is concentrated at relatively low values,

while a long right tail corresponds to regimes or contracts characterized by unusually low realized volatility. These extreme realizations arise endogenously from the volatility-scaling mechanism itself and do not primarily reflect structural market dislocations or persistent risk premia.

From a modeling perspective, this feature is consequential. Linear specifications that treat volatility-scaled exposure as approximately proportional to changes in volatility may fail to capture the asymmetric response of leverage across regimes. Flexible non-linear architectures are better suited to accommodate the threshold-like behavior induced by volatility targeting, especially in settings where exposure amplification during low-volatility periods magnifies the effect of predictive signals, while exposure compression during high-volatility episodes dampens their impact.

The learning target is constructed as the volatility-scaled next-period return,

$$\text{target}_t = \text{clip}\left(\frac{r_{t+1}}{\sigma_t}, -20, 20\right), \quad (23)$$

where clipping is applied to limit the influence of extreme realizations during training.

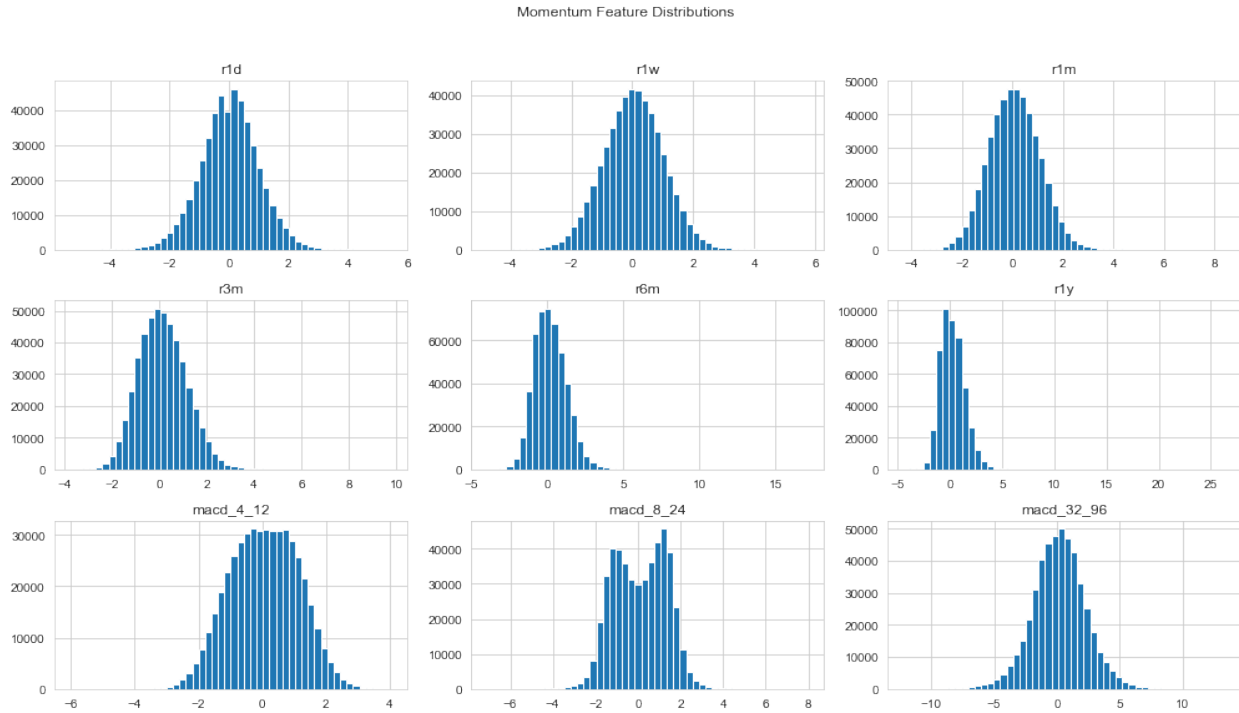


Figure 6: Distribution of Momentum Features.

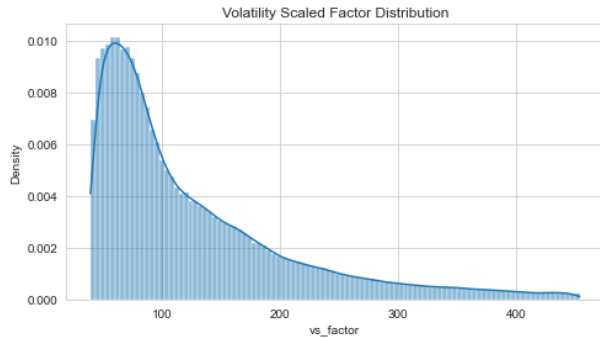


Figure 7: Induced Exposure by Volatility Targeting.

## A.6 Stylized Facts of Returns and Volatility

Daily returns exhibit strong deviations from Gaussianity, with heavy tails and excess kurtosis that imply substantial downside risk and state dependence. Realized volatility is highly skewed and persistent, re-

flecting clustering and regime-dependent risk dynamics. These features challenge linear predictive models that rely on homoskedastic or symmetric error assumptions.

## A.7 Formal Statistical Diagnostics

To formally substantiate the distributional characteristics suggested by the graphical evidence, we conduct standard diagnostic tests.

First, normality of returns is rejected at conventional significance levels using the Jarque–Bera test across the majority of instruments, consistent with the heavy tails observed in Figure 5. Excess kurtosis and skewness statistics further confirm substantial deviations from Gaussianity.

Second, we test for non-stationarity in price levels using augmented Dickey–Fuller tests. As expected for financial price series, unit roots cannot generally be rejected in levels, while returns exhibit stationar-

ity. This is consistent with the standard representation of asset prices as integrated processes with stationary increments.

Third, volatility persistence is assessed via autocorrelation of squared returns and realized volatility. We observe slow decay in the autocorrelation function, confirming volatility clustering and regime dependence.

Taken together, these diagnostics confirm that the dataset exhibits canonical stylized facts of financial time series: heavy tails, conditional heteroskedasticity, and non-stationarity in levels.

## A.8 Implications for Modeling

Taken together, the distributional evidence highlights a fundamental feature of the data. While the input predictors are largely bounded, symmetric, and well-behaved, the target variable—realized returns—exhibits extreme kurtosis, heavy tails, and strong state dependence. This mismatch implies that the primary modeling challenge lies not in stabilizing the inputs, but in accurately capturing the conditional distribution of returns given these inputs.

These empirical properties motivate the use of flexible nonlinear architectures that can accommodate interactions, threshold effects, and regime-dependent behavior. Nonlinear dependencies and regime changes are frequently observed in financial time series and are captured most effectively by nonlinear models [39]. Neural network architectures such as LSTMs have shown superior performance in capturing complex nonlinear patterns in volatility and return dynamics [40]. In environments where small changes in predictors can, under certain conditions, lead to disproportionately large changes in outcomes, models that adapt their functional form across the state space are particularly well suited.

## A.9 Scope and External Validity

While the dataset exhibits statistical properties commonly observed in financial markets, the conclusions drawn in this study are, strictly speaking, conditional on the data considered. As with any empirical investigation, it is not possible to establish universal

generality beyond the sampled instruments and time period.

That said, the presence of heavy-tailed returns, volatility clustering, and regime-dependent dynamics suggests that the dataset captures structural characteristics typical of many financial time series. For this reason, we view the benchmark as representative of a broad class of cross-asset forecasting problems. Nevertheless, extending the analysis to alternative markets, frequencies, or macroeconomic environments remains an important direction for future research.

# B Architecture Components

## B.1 Linear Baselines

**Autoregressive Model (AR1x).** We consider an AR(1) process

$$y_t = \phi y_{t-1} + \varepsilon_t, \quad \varepsilon_t \sim \mathcal{N}(0, \sigma^2), \quad (24)$$

which captures short-term autocorrelation. This model assumes 1 one input feature. AR1x simply applies AR(1) to each feature independently (for multiple input features).

**DLinear and NLinear.** DLinear and NLinear [15] apply linear mappings to the input window:

$$\hat{y}_t = W\mathbf{X}_t + b. \quad (25)$$

DLinear decomposes the input into trend and seasonal components, while NLinear operates on normalized inputs. Both models lack temporal state and serve as non-recurrent linear baselines.

## B.2 Transformer Background

Transformer architectures [1] compute self-attention quadratically as

$$\text{Attn}(Q, K, V) = \text{softmax}\left(\frac{QK^\top}{\sqrt{d_k}}\right)V. \quad (26)$$

Therefore, Transformer-based models have a large number of trainable parameters.

### B.3 State-Space Model Details

Mamba models [6, 29] implement selective state-space models of the form

$$h_t = A_t h_{t-1} + B_t x_t, \quad y_t = C_t h_t, \quad (27)$$

where  $h_t$  denotes the latent state,  $x_t$  the input, and  $y_t$  the output. The matrices  $A_t$ ,  $B_t$ , and  $C_t$  are initialized using HiPPO LegS matrices [8], which provide a principled discretization of continuous-time linear dynamical systems.

In Mamba2, the state transition matrix is replaced with a scaled identity, and the architecture incorporates a form of linear attention [7], improving efficiency and numerical stability.

In this work, we employ a static HiPPO transition matrix and a fixed low-rank parameterization of the step size  $\Delta$ , resulting in a fixed temporal horizon. This modification reduces sensitivity to noise and improves robustness when modeling financial time series.

### B.4 LSTM-based models

The LSTM architecture is included as a canonical gated recurrent model that addresses the vanishing gradient limitations of standard RNNs through an additive memory cell and multiplicative gating. The forget and input gates enable adaptive control over memory retention and update, effectively implementing a data-dependent filtering mechanism.

The LSTM [11] updates are given by

$$f_t = \sigma(W_f x_t + U_f h_{t-1} + b_f), \quad (28)$$

$$i_t = \sigma(W_i x_t + U_i h_{t-1} + b_i), \quad (29)$$

$$o_t = \sigma(W_o x_t + U_o h_{t-1} + b_o), \quad (30)$$

$$c_t = f_t \odot c_{t-1} + i_t \odot \tanh(W_c x_t), \quad (31)$$

$$h_t = o_t \odot \tanh(c_t), \quad (32)$$

where  $f_t$ ,  $i_t$ , and  $o_t$  denote the forget, input, and output gates, respectively. Such adaptive memory is particularly relevant in financial time series, where structural breaks and regime shifts render fixed-memory models suboptimal. The gating mechanism allows the model to dynamically adjust the effective time horizon over which past information is retained.

Moreover, the nonlinear hidden-state representation provides a flexible mechanism for extracting predictive structure from low signal-to-noise and non-Gaussian data, making LSTMs a natural and widely adopted baseline in financial forecasting tasks.

**xLSTM.** We provide a concise technical description of xLSTM following [12] (Eq. 8–17).

**Exponential Gating.** In contrast to classical LSTMs, which employ sigmoid gates  $f_t = \sigma(\cdot)$  and  $i_t = \sigma(\cdot)$ , xLSTM replaces sigmoid activations with exponential gating followed by normalization. Let

$$\tilde{f}_t = W_f x_t + R_f h_{t-1} + b_f, \quad (33)$$

$$\tilde{i}_t = W_i x_t + R_i h_{t-1} + b_i, \quad (34)$$

which are the pre-activation gates, similar to LSTM. The raw gates are exponentiated,

$$\hat{f}_t = \exp(\tilde{f}_t), \quad \hat{i}_t = \exp(\tilde{i}_t), \quad (35)$$

and subsequently normalized to ensure numerical stability and controlled memory growth. In log-domain form, this normalization is implemented via a running maximum term to prevent overflow (see [12], Eq. 15–17). The resulting gates satisfy a convex combination structure analogous to classical LSTM gating but without sigmoid saturation.

**sLSTM (Scalar LSTM).** The scalar variant maintains a single memory state per unit. The update equations are

$$\tilde{c}_t = \tanh(W_z x_t + R_z h_{t-1} + b_z), \quad (36)$$

$$c_t = f_t \odot c_{t-1} + i_t \odot \tilde{c}_t, \quad (37)$$

$$n_t = f_t \odot n_{t-1} + i_t, \quad (38)$$

$$h_t = o_t \odot \frac{c_t}{n_t}, \quad (39)$$

where  $f_t$ ,  $i_t$ , and  $o_t$  denote normalized exponential forget, input, and output gates, respectively, and  $n_t$  is a stabilizing normalizer. The division by  $n_t$  ensures scale control of the memory state.

**mLSTM (Matrix LSTM).** The matrix variant generalizes the memory to a matrix-valued state  $C_t \in \mathbb{R}^{d \times d}$ . At each step, key-value vectors  $k_t, v_t \in \mathbb{R}^d$  are generated and stored via a gated outer-product update:

$$C_t = f_t \odot C_{t-1} + i_t \odot (v_t k_t^\top). \quad (40)$$

The hidden state is retrieved through a query vector  $q_t$ ,

$$h_t = C_t q_t, \quad (41)$$

This Bidirectional Associative Memory (BAM) [41–44] setting yields high separability between stored patterns and allows efficient recall of past information. Importantly, mLSTM removes state compression recurrence but still has temporal dependency in memory accumulation. It is more parallelizable, but not fully parallel.

**Patch sLSTM (PsLSTM).** Given a multivariate time series  $X \in \mathbb{R}^{L \times d}$ , each channel is treated independently and segmented into non-overlapping patches of length  $\ell$ :

$$\tilde{x}_p^{(i)} = \text{Patch} \left( x_{(p-1)\ell+1:p\ell}^{(i)} \right), \quad i = 1, \dots, d. \quad (42)$$

Each patch embedding is processed by an sLSTM with shared parameters across channels:

$$h_p^{(i)} = \text{sLSTM}(h_{p-1}^{(i)}, \tilde{x}_p^{(i)}). \quad (43)$$

Parameter sharing preserves channel independence while reducing model complexity and mitigating overfitting.

## B.5 Hybrid Architecture Details

The hybrids are designed to improve robustness in noisy financial time series by enhancing the signal-to-noise ratio, enabling adaptive feature selection, and stabilizing temporal state updates.

**Variable Selection Network (VSN)** The Variable Selection Network (VSN), inspired by the Temporal Fusion Transformer [5], performs feature-wise nonlinear embedding followed by dynamic soft selection of relevant covariates at each time step.

Given an input vector  $x_t \in \mathbb{R}^C$  consisting of  $C$  covariates, each variable is embedded independently:

$$h_{t,i} = \phi_i(x_{t,i}), \quad i = 1, \dots, C, \quad (44)$$

where  $\phi_i(\cdot)$  denotes a learnable nonlinear embedding function.

The embeddings are concatenated and passed through a gating network to compute feature importance weights:

$$\alpha_t = \text{softmax}(W_g[h_{t,1}, \dots, h_{t,C}] + b_g), \quad (45)$$

where  $W_g$  and  $b_g$  are learnable parameters.

The selected representation is computed as a weighted sum:

$$\tilde{x}_t = \sum_{i=1}^C \alpha_{t,i} h_{t,i}. \quad (46)$$

This mechanism enables adaptive suppression of noisy or uninformative covariates and improves robustness in non-stationary environments.

**VSN+LSTM (VLSTM)** The VSN+LSTM (VLSTM) model combines VSN-based feature selection with recurrent temporal encoding. At each time step, the input vector is processed by a VSN to produce a dynamically weighted feature representation:

$$\tilde{x}_t = \text{VSN}(x_t). \quad (47)$$

The resulting sequence  $\{\tilde{x}_t\}_{t=1}^L$  is then passed through an LSTM to construct a compact temporal state:

$$(h_t, c_t) = \text{LSTM}(\tilde{x}_t, h_{t-1}, c_{t-1}). \quad (48)$$

For one-step-ahead forecasting, the prediction is obtained from the final hidden state:

$$\hat{y}_{L+1} = W_o h_L + b_o. \quad (49)$$

**VSN–Mamba2** In the VSN–Mamba2 hybrid, feature selection and temporal modeling are explicitly decoupled. Given an input  $x_t \in \mathbb{R}^d$ , the VSN computes feature-wise importance weights:

$$\alpha_t = \text{softmax}(g(x_t)), \quad \tilde{x}_t = \alpha_t \odot x_t, \quad (50)$$

where  $g(\cdot)$  denotes a learnable gating network and  $\odot$  denotes element-wise multiplication.

The filtered input  $\tilde{x}_t$  is then passed to the Mamba2 state-space block:

$$h_t = Ah_{t-1} + B\tilde{x}_t, \quad (51)$$

where  $A$  and  $B$  denote the state transition and input matrices, respectively. This design improves robustness by reducing the influence of noisy covariates prior to temporal state updates.

**LSTM + PatchTST** This hybrid architecture combines explicit recurrence with attention by using an LSTM as a channel-wise temporal denoiser prior to PatchTST. Each input channel is processed independently using a shared LSTM backbone:

$$h_t^{(i)} = \text{LSTM}(x_t^{(i)}, h_{t-1}^{(i)}), \quad i = 1, \dots, d, \quad (52)$$

where  $x_t^{(i)}$  denotes the  $i$ -th feature.

The resulting hidden states are segmented into temporal patches and passed to PatchTST, which applies self-attention over patches:

$$\tilde{h}_p = \text{PatchTST}(\{h_t^{(i)}\}_{t \in \mathcal{P}_p}), \quad (53)$$

where  $\mathcal{P}_p$  denotes the set of time steps belonging to patch  $p$ .

This separation of concerns allows the LSTM to stabilize local temporal structure while PatchTST aggregates medium- and long-range dependencies.

**VSN + xLSTM** In the VSN + xLSTM hybrid, the sequence of VSN-selected representations is directly fed into an xLSTM. The model maintains a matrix-valued memory state  $M_t \in \mathbb{R}^{H \times H}$ , which is updated recursively:

$$(M_t, s_t) = \text{xLSTM}(\tilde{x}_t, M_{t-1}), \quad (54)$$

where  $s_t \in \mathbb{R}^H$  denotes the output state. The matrix-valued memory enables modeling of higher-order temporal interactions and long-range dependencies beyond the capacity of vector-based recurrent architectures.

## B.6 Temporal Fusion Transformer Details

TFT combines recurrent encoding with attention-based aggregation. Given an input sequence  $\{x_t\}_{t=1}^L$ , a recurrent encoder produces latent states

$$h_t = \text{LSTM}(x_t, h_{t-1}).$$

Multi-head attention is then applied to aggregate information across time:

$$\hat{y}_t = \text{Attn}(h_{1:t}).$$

Variable selection networks, gating layers, and static covariate encoders further modulate the representations to improve interpretability and robustness.

## C Model Configurations and Hyperparameter Selection

To ensure a fair and systematic comparison across architectures, we define structured hyperparameter search spaces tailored to each model family. All models are evaluated under comparable training budgets, with architecture-specific parameters varied only where structurally relevant. Tables 6 and 7 summarizes the general configuration ranges.

**General Training Configuration.** For each model, we tune the batch size, hidden dimensionality ( $H$ ), learning rate, and input sequence length. Learning rates are selected from logarithmic ranges between  $10^{-4}$  and  $10^{-2}$  or from discrete sets  $\{10^{-3}, 5 \times 10^{-4}, 10^{-4}\}$  depending on architectural stability. Sequence lengths are chosen to reflect short- and medium-horizon dependencies (e.g., 64–512 timesteps), while maintaining comparability across models.

**Architecture-Specific Hyperparameters.** In addition to shared training parameters, each model family includes structural hyperparameters:

- **Transformer-based models** (e.g., TFT, PatchTST) vary the number of attention heads, encoder layers, and sparsity factors.
- **State-space models** (Mamba2 variants) tune the number of layers, convolution kernel size, SSM expansion factors, rank, and discretization parameters (e.g.,  $\Delta_{\max}$ , HiPPO scaling).
- **xLSTM-based models** vary the number of stacked blocks, convolutional kernel sizes, and projection expansion factors.
- **Patch-based models** additionally tune patch length and stride fraction.
- **Classical baselines** (AR1, DLinear) are evaluated with minimal architectural tuning.

**Search Protocol.** Hyperparameter selection is performed via grid search over the predefined discrete ranges. Each configuration is trained independently, and the best-performing setting is selected based on validation Sharpe Ratio. Importantly, the same validation procedure and performance metric are used for all architectures to avoid selection bias.

**Training Details.** We employ the ADAM optimizer [45] for all models. Early stopping is applied with a patience of 20 epochs. For validation, the last 10% of the training data is reserved as a validation set. Gradient clipping based on the gradient norm is used to stabilize training.

Models are retrained every five years using a rolling-window scheme. For strategies requiring an initial lookback period, performance metrics such as the Sharpe ratio are not evaluated during the burn-in phase. In particular, for models with a fixed initialization window we use  $L_0 = 21$ , while for sequence models the burn-in period corresponds to one quarter of the input sequence length (e.g., 21 for sequence length 84 and 128 for sequence length 512).

**Model Capacity Considerations.** The number of trainable parameters varies substantially across models (Table 6), reflecting inherent architectural differences. We do not explicitly match parameter counts, as doing so would distort the native design of certain architectures (e.g., state-space vs. attention-based models). Instead, we control for training protocol, optimization strategy, and evaluation metric to ensure comparability.

This structured configuration framework ensures that performance differences arise from architectural properties rather than inconsistent tuning practices.

## D Performance Metrics and Evaluation Criteria

This appendix describes the performance, risk, and robustness measures used throughout the empirical evaluation. Given the low signal-to-noise ratio and heavy-tailed nature of financial returns, we rely on a broad set of complementary metrics to assess not only average performance, but also statistical significance, downside risk, trading intensity, and incremental value relative to a passive benchmark.

### D.1 Return and Risk-Adjusted Performance

**Annualized Return.** Annualized return is computed as the mean daily portfolio return scaled by the number of trading days per year. While intuitive, this metric does not account for risk and is therefore interpreted jointly with risk-adjusted measures.

**Compound Annual Growth Rate (CAGR).** CAGR measures the geometric average annual growth of portfolio value over the evaluation period:

$$\text{CAGR} = \left( \frac{V_T}{V_0} \right)^{1/T} - 1,$$

where  $V_0$  and  $V_T$  denote initial and terminal portfolio values and  $T$  is the length of the sample in years. CAGR reflects long-run capital accumulation and penalizes volatility drag.

Table 6: Model configurations and general hyperparameter search ranges.

Model	Trainable Params	Batch Size	Hidden Dim (H)	LR Range	Seq Len	Dropout
Mamba2+VSN	3,571,348	{32,64,128}	{32,64,128,256}	$10^{-4}$ – $10^{-2}$	84	{0.1,0.2,0.3,0.4}
xLSTM	2,507,269	{128,256}	{64,128,256}	{1e-3,5e-4,1e-4}	84	{0.2,0.3,0.4,0.5}
xLSTM+VSN	6,146,368	{128,256}	{64,128,256}	{1e-3,5e-4,1e-4}	84	{0.2,0.3,0.4,0.5}
PsLSTM	1,963,841	{16,32}	{16,32,64}	{1e-3,5e-4,1e-4}	512	{0.2,0.3,0.4,0.5}
VLSTM	1,142,963	{128,256}	{64,128,256}	$10^{-4}$ – $10^{-2}$	84	{0.2,0.3,0.4,0.5}
LSTM	73,729	{128,256}	{64,128,256}	$10^{-4}$ – $10^{-2}$	84	{0.2,0.3,0.4,0.5}
PatchTST	1,139,739	{16,32}	{16,32,64,96}	{1e-3,5e-4}	512	{0.1,0.2,0.3,0.4,0.5}
LSTM+PatchTST	634,881	{16,32}	{16,32,64,96}	{1e-3,5e-4}	512	{0.1,0.2,0.3,0.4,0.5}
Mamba2	18,882	{32,64,128}	{32,64,128,256}	$10^{-4}$ – $10^{-2}$	84	{0.1,0.2,0.3,0.4}
DLinear	2,111	{256,512,1024}	{64,128,256}	$10^{-4}$ – $10^{-2}$	64	{0.1,0.2,0.3}
AR1	2,073	{128,256}	{64,128,256}	$10^{-4}$ – $10^{-2}$	84	{0.2,0.3,0.4,0.5}
TFT	347,507	{128,256}	{64,128,256}	$10^{-4}$ – $10^{-2}$	84	{0.2,0.3,0.4,0.5}

Table 7: Architecture-specific hyperparameter search spaces.

Architecture	Hyperparameter Search Space
Transformer-based	Heads: {1,2,4}; Layers: {3,4,5,6}; Sparsity: {2,3,4,5,6}
Mamba / SSM	Layers: {1,2,3,5}; Kernel: {2,3,5,7,9}; Conv: {2,8,16,32}
xLSTM	Rank: {4,8,16,32}; $\Delta_{\max}$ : {0.2,0.4,0.6,0.8}; HiPPO: 0.1–0.5
Patch-based	Blocks: {1–6}; Kernel: {1,2,4,6,7,9}; Projection: {1–2.5}
Classical (AR1, DLinear)	Patch Length: {4,8,16,32,64}; Stride: {0.25,0.5,1}
	Layers: {2,3,5}

**Sharpe Ratio.** The Sharpe ratio is defined as the mean excess return divided by the standard deviation of returns. All reported Sharpe ratios are annualized. This is the primary optimization objective and headline performance metric throughout the study.

**Information Ratio.** The Information Ratio measures risk-adjusted excess performance relative to a passive buy-and-hold benchmark:

$$\text{IR} = \frac{\hat{\mathbb{E}}[r_t - r_t^{\text{passive}}]}{\sqrt{\hat{\text{Var}}(r_t - r_t^{\text{passive}})}}.$$

This metric captures incremental value beyond market exposure.

## D.2 Statistical Significance

**HAC-Adjusted  $t$ -Statistics.** To assess statistical significance under serial correlation and heteroskedasticity, we report Newey–West heteroskedasticity and autocorrelation consistent (HAC)  $t$ -statistics for mean returns and Sharpe ratios. This adjustment is critical in financial time series, where returns often exhibit time dependence.

**HAC  $t$ -Statistic versus Passive.** We additionally report HAC-adjusted  $t$ -statistics for excess returns relative to the passive benchmark, testing whether observed outperformance is statistically distinguishable from zero after accounting for dependence in relative returns.

### D.3 Directional Accuracy and Trading Activity

**Hit Rate.** The hit rate measures the fraction of periods in which the strategy correctly predicts the sign of returns. While not sufficient for profitability on its own, it provides insight into directional consistency.

**Turnover.** Turnover is defined as the average absolute change in portfolio weights across consecutive periods. High turnover implies greater transaction costs and reduced implementability.

**Turnover (xGMV).** Turnover expressed as a multiple of gross market value (xGMV) provides a scale-free measure of trading intensity and facilitates comparison across strategies.

### D.4 Downside Risk and Tail Behavior

**Maximum Drawdown.** Maximum drawdown is the largest peak-to-trough decline in cumulative portfolio value. It captures worst-case capital loss and is a key risk metric for real-world deployment.

**Calmar Ratio.** The Calmar ratio is defined as CAGR divided by maximum drawdown. It measures return efficiency relative to extreme downside risk and complements the Sharpe ratio.

**Conditional Value-at-Risk (CVaR 5%).** CVaR at the 5% level measures the expected loss conditional on returns falling in the worst 5% of outcomes. Unlike Value-at-Risk, CVaR captures tail severity and is particularly relevant in heavy-tailed financial return distributions.

### D.5 Benchmark-Relative Diagnostics

**Correlation versus Passive.** We report the Pearson correlation between strategy returns and the passive benchmark. Lower correlation indicates greater diversification benefits and reduced dependence on market direction.

**Profit and Loss (PnL).** Cumulative profit and loss (PnL) curves are used for visual comparison of strategies over time. PnL trajectories provide insight into path dependence, drawdown behavior, and regime sensitivity that may not be evident from summary statistics alone.

Taken together, these metrics provide a comprehensive and economically meaningful assessment of model performance, balancing average returns, statistical reliability, downside risk, trading realism, and incremental value over a passive investment strategy.

## E Asset-level Results

This section provides a detailed breakdown of model performance at the individual asset level. The per-asset analysis presented here serves two purposes: (i) to evaluate cross-sectional robustness and (ii) to assess whether performance is concentrated in specific asset classes or broadly distributed across markets.

We use *breakeven transaction cost*, which is defined as the constant cost per unit of leveraged turnover that drives total gross PnL to zero. Formally,

$$c^* = \frac{\sum_t R_t^{\text{gross}}}{\sum_t \tau_t},$$

where  $\tau_t$  denotes leveraged turnover. If actual trading costs remain below  $c^*$ , the strategy remains profitable; the ratio  $c^*/c_{\text{actual}}$  measures implementation robustness.

Results are grouped by asset category (Bond, Commodity, Energy, FX, and Index futures). For each model, we report cumulative PnL trajectories per asset as well as box-and-whisker summaries of the Sharpe Ratio distributions. This allows us to examine both temporal consistency and cross-sectional dispersion.

### E.1 Asset Description

Table 8 reports the full universe of tradable assets included in the empirical analysis. The cross-asset dataset spans foreign exchange, equity indices, fixed income, energy, and agricultural and metal commodities, including both pit and electronic contracts

Table 8: Asset universe and classification.

Ticker	Group	Description	Ticker	Group	Description	Ticker	Group	Description
AN	FX	Australian dollar comp	BC	Energy	Brent crude oil	BG	Energy	Brent gasoil
BN	FX	British pound comp	CA	Index	CAC 40 index	CADJPY	FX	CAD JPY cross
CB	Bond	Canada 10Y bond	CC	Comdty	Cocoa	CN	FX	Canadian dollar comp
CR	Comdty	CRB index	CT	Comdty	Cotton No.2	DA	Comdty	Milk III
DT	Bond	Euro Bund	DX	FX	US dollar index	EN	Index	Nasdaq mini
ER	Index	Russell 2000 mini	ES	Index	S&P 500 mini	FB	Bond	US 5Y note comp
FN	Index	Euro Stoxx comp	GI	Comdty	Goldman Sachs idx	GS	Bond	UK Gilt long
HS	Index	Hang Seng	JN	FX	Japanese yen comp	JO	Comdty	Orange juice
KC	Comdty	Coffee	KW	Comdty	Wheat KC	LB	Comdty	Lumber
LX	Index	FTSE 100	MD	Index	S&P 400 mini	MP	FX	Mexican peso
MW	Comdty	Wheat Minneapolis	NK	Index	Nikkei 225	NOKUSD	FX	NOK USD cross
NR	Comdty	Rough rice	SB	Comdty	Sugar No.11	SN	FX	Swiss franc comp
TU	Bond	US 2Y note comp	TY	Bond	US 10Y note comp	UB	Bond	Euro Bobl
US	Bond	US T-bond comp	USDNZD	FX	USD NZD cross	USDSEK	FX	USD SEK cross
USDSGD	FX	USD SGD cross	UZ	Bond	Euro Schatz	XU	Index	Euro Stoxx 50
XX	Index	STOXX 50	YM	Index	Mini Dow	ZA	Comdty	Palladium elec
ZB	Energy	RBOB elec	ZC	Comdty	Corn elec	ZF	Comdty	Feeder cattle elec
ZG	Comdty	Gold elec	ZI	Comdty	Silver elec	ZK	Comdty	Copper elec
ZL	Comdty	Soybean oil elec	ZM	Comdty	Soybean meal elec	ZN	Energy	Natural gas elec
ZO	Comdty	Oats elec	ZP	Comdty	Platinum elec	ZR	Comdty	Rough rice elec
ZS	Comdty	Soybeans elec	ZT	Comdty	Live cattle elec	ZU	Energy	Crude oil elec
ZW	Comdty	Wheat elec	ZZ	Comdty	Lean hogs elec			

where available. This broad coverage ensures substantial cross-sectional and cross-asset heterogeneity, enabling the evaluation of model robustness across diverse liquidity conditions, macroeconomic exposures, and volatility regimes.

## E.2 VSLTM

Figures 8–12 display cumulative PnL per asset across the five asset categories. The corresponding box-and-whisker plots (Figures 13–17) summarize the distribution of Sharpe Ratio for each instrument.

Several observations emerge. First, performance is not driven by a single dominant contract but is distributed across multiple assets within each category. Second, tail behavior, as captured in the box plots, suggests that risk-adjusted performance is primarily driven by stable median returns rather than isolated extreme gains.

Overall, the per-asset analysis indicates that VLSTM’s aggregate performance is supported by consistent cross-sectional contributions rather than concentration in a small subset of instruments.

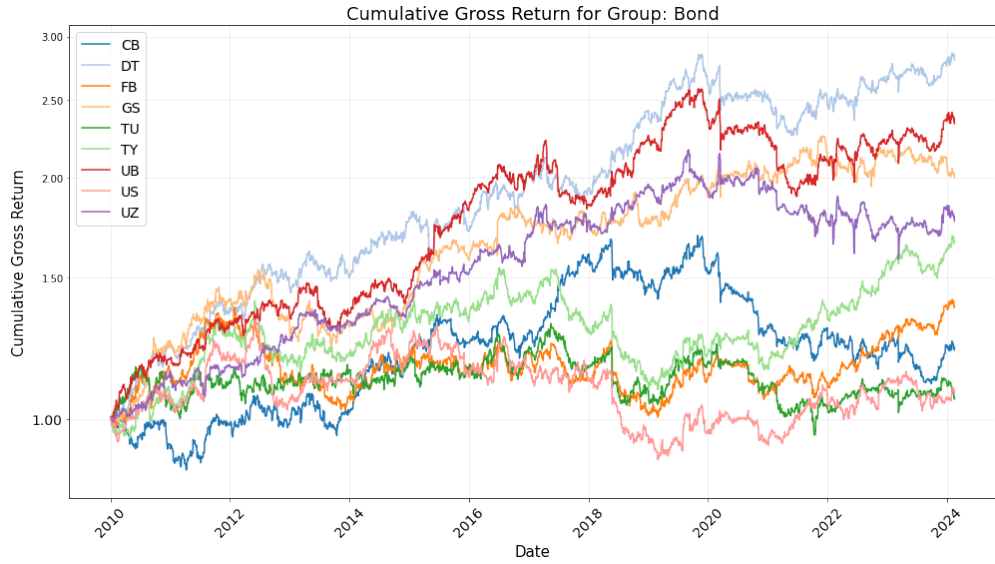


Figure 8: VLSTM PnL per asset - bond Futures

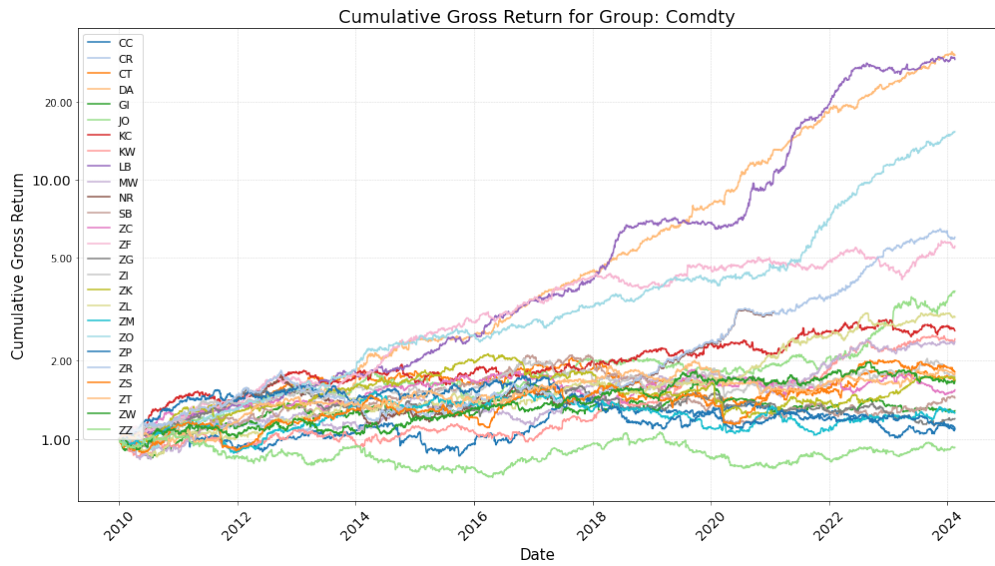


Figure 9: VLSTM PnL per asset - Commodities Futures

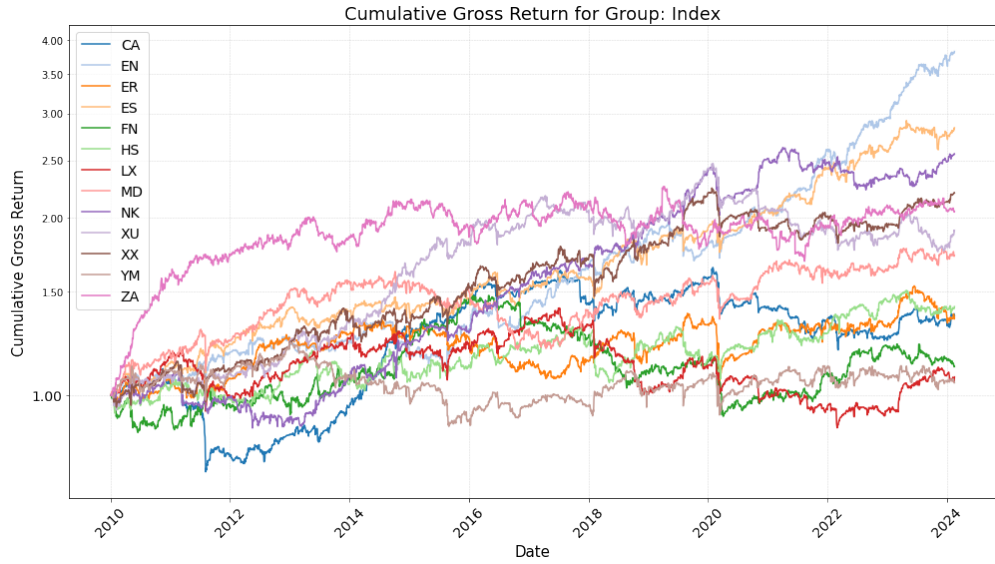


Figure 10: VLSTM PnL per asset - Index Futures

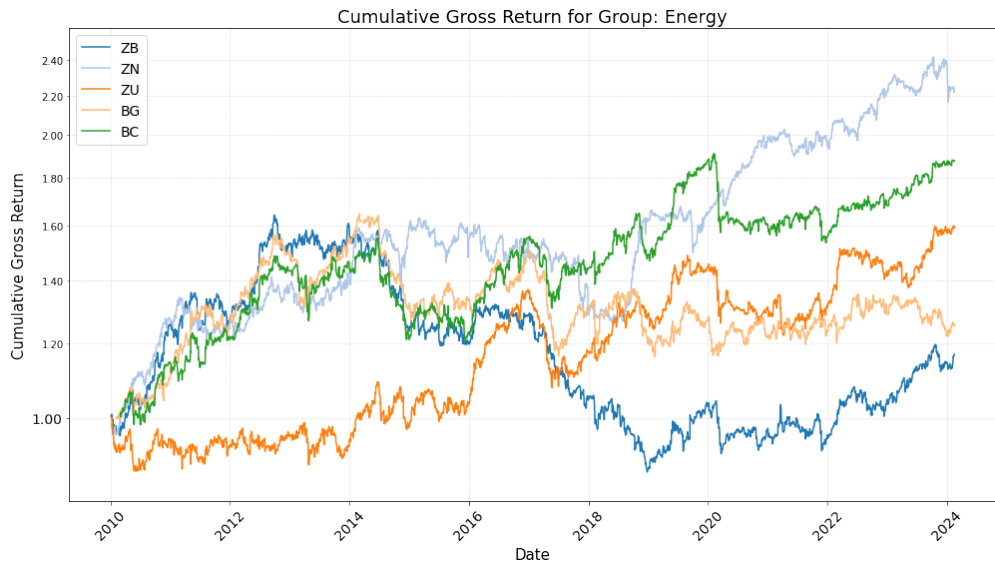


Figure 11: VLSTM PnL per asset - Energy Futures

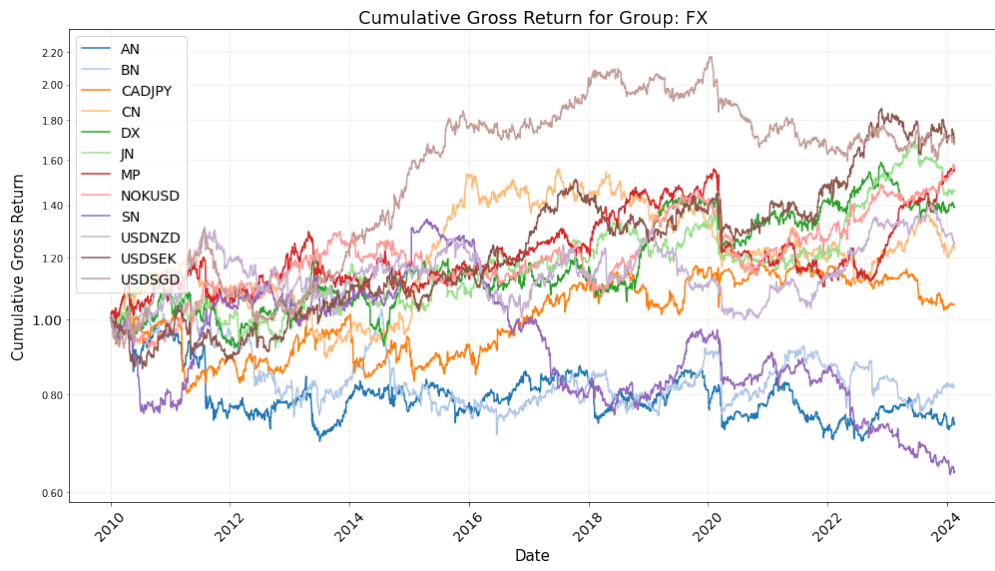


Figure 12: VLSTM PnL per asset - FX Futures

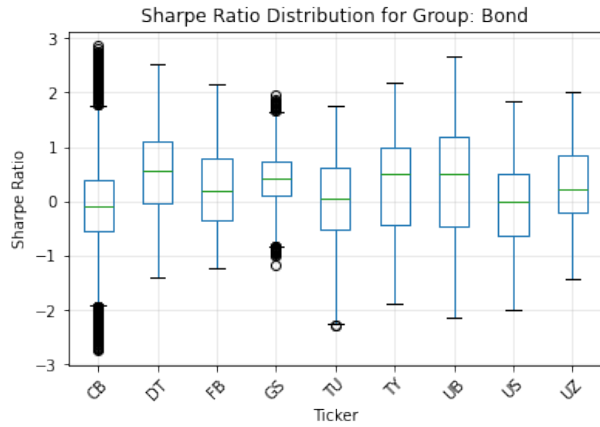


Figure 13: VLSTM box and whisker annual Sharpe Ratio per asset - Bond Futures

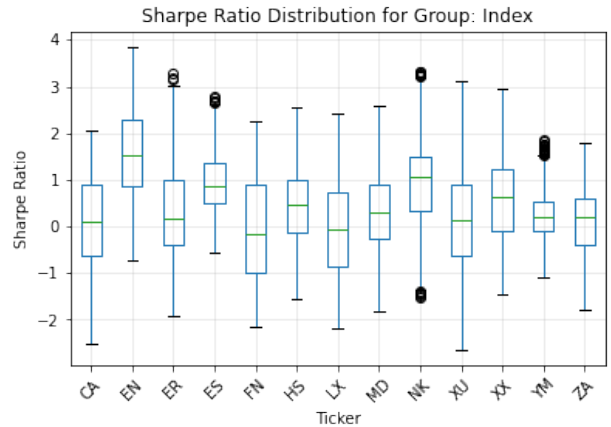


Figure 15: VLSTM box and whisker annual Sharpe Ratio per asset - Index Futures

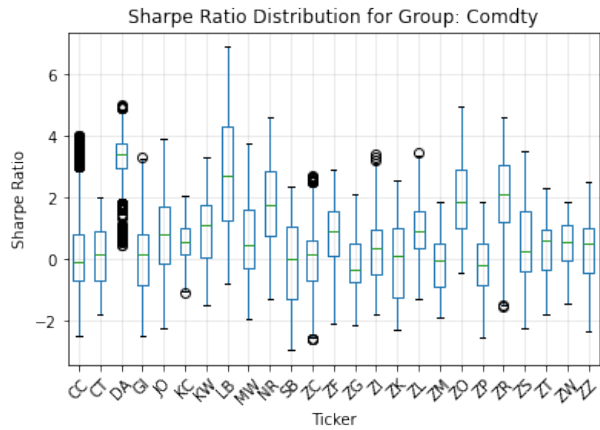


Figure 14: VLSTM box and whisker annual Sharpe Ratio per asset - Commodities Futures

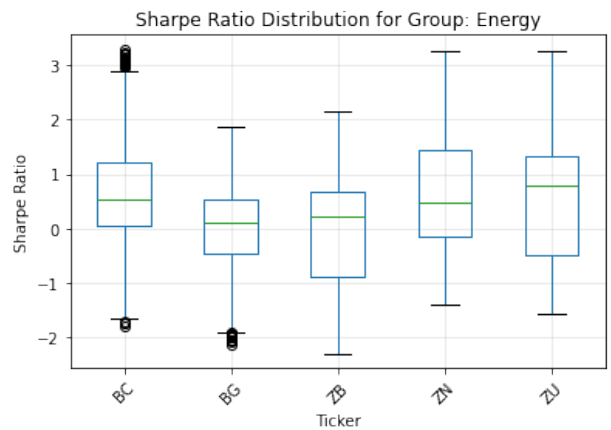


Figure 16: VLSTM box and whisker annual Sharpe Ratio per asset - Energy Futures

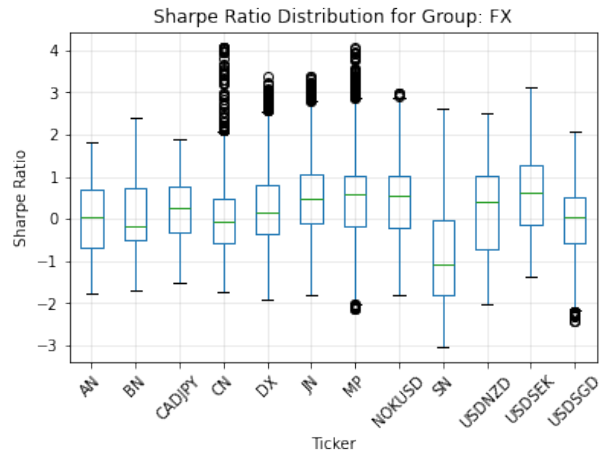


Figure 17: VLSTM box and whisker annual Sharpe Ratio per asset - FX Futures

Table 9: VLSTM: Annualised Volatility-Rescaled Performance and Breakeven Transaction Costs (bps)

Ticker	Gross (ann.)	Turnover (ann.)	$c^*$ (bps)	Ticker	Gross (ann.)	Turnover (ann.)	$c^*$ (bps)
LB	0.2485	80.58	30.84	ZO	0.2027	84.01	24.13
DA	0.2529	114.78	22.04	ZN	0.0618	45.04	13.73
JO	0.0986	74.19	13.29	EN	0.1003	86.69	11.57
KC	0.0738	63.92	11.54	ZR	0.1339	137.44	9.75
BC	0.0512	61.26	8.36	ZF	0.1279	157.12	8.14
NR	0.1086	137.78	7.88	NK	0.0706	89.77	7.87
ES	0.0796	107.12	7.43	KW	0.0686	93.77	7.32
ZL	0.0827	115.79	7.15	ZA	0.0558	82.87	6.74
ZI	0.0444	68.93	6.44	ZU	0.0381	64.42	5.91
ZS	0.0476	83.69	5.68	MW	0.0669	127.30	5.25
XU	0.0507	98.17	5.17	XX	0.0614	118.76	5.17
ZK	0.0421	83.07	5.06	CT	0.0421	91.73	4.59
ZW	0.0417	91.08	4.57	SB	0.0313	80.33	3.89
MD	0.0442	115.53	3.82	HS	0.0301	85.51	3.52
ZC	0.0363	103.71	3.50	ZT	0.0464	135.72	3.42
ER	0.0264	80.13	3.30	CA	0.0267	92.21	2.90
CR	0.0389	138.25	2.82	BG	0.0216	78.91	2.73
DT	0.0782	291.86	2.68	MP	0.0368	143.21	2.57
ZM	0.0215	83.55	2.57	GI	0.0230	94.01	2.44
ZB	0.0160	66.47	2.41	NOKUSD	0.0382	165.09	2.31
USDSEK	0.0419	188.00	2.23	GS	0.0547	282.39	1.94
JN	0.0321	209.92	1.53	ZG	0.0177	119.59	1.48
CC	0.0115	78.16	1.47	USDNZD	0.0209	169.47	1.23
USDSGD	0.0422	368.09	1.15	UB	0.0664	591.04	1.12
ZP	0.0110	101.90	1.08	TY	0.0415	411.13	1.01
DX	0.0284	298.04	0.95	LX	0.0101	109.94	0.91
YM	0.0085	106.28	0.80	CN	0.0199	272.83	0.73
CB	0.0194	344.26	0.56	FN	0.0130	233.13	0.56
CADJPY	0.0080	151.64	0.53	US	0.0104	198.09	0.52
FB	0.0281	689.19	0.41	UZ	0.0508	1940.20	0.26
TU	0.0094	2218.65	0.04	ZZ	-0.0004	80.57	-0.05
BN	-0.0092	207.76	-0.44	AN	-0.0170	164.71	-1.03
SN	-0.0272	212.34	-1.28				

### E.3 xLSTM

Figures 18–22 present cumulative PnL per asset for xLSTM across the five asset groups. The associated box-and-whisker plots (Figures 23–27) provide distributional summaries.

Relative to VLSTM, xLSTM exhibits stronger cross-sectional homogeneity in certain categories. In higher-volatility sectors such as energy and commodities, dispersion increases, but median performance remains positive across most instruments. This suggests that the model adapts to heterogeneous volatility structures without excessive tail risk concentration.

Importantly, no systematic degradation is observed in a specific asset class, indicating that performance is not regime- or sector-dependent. The cross-asset consistency observed in the box plots further supports the robustness of the learned representations.

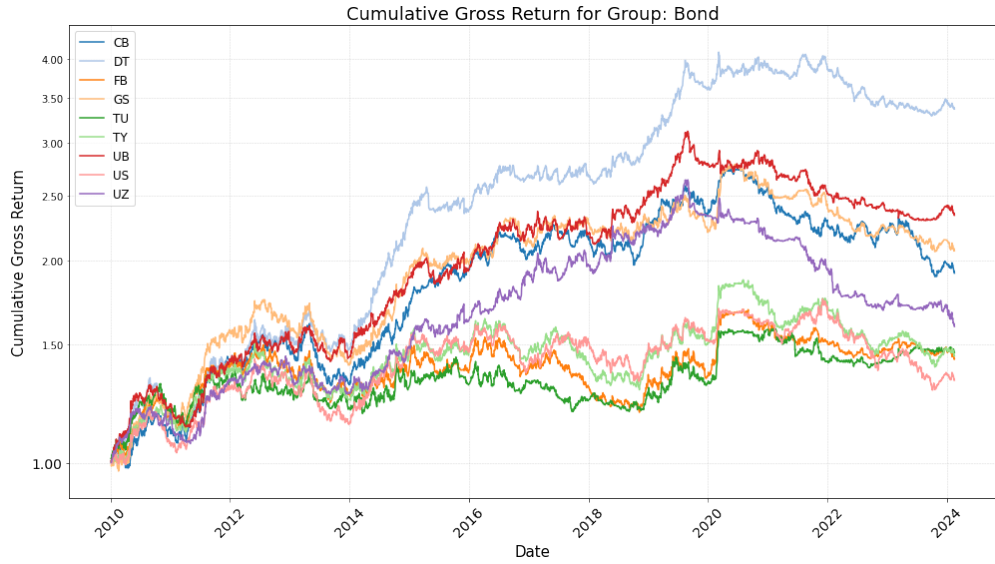


Figure 18: xLSTM PnL per asset - bond Futures

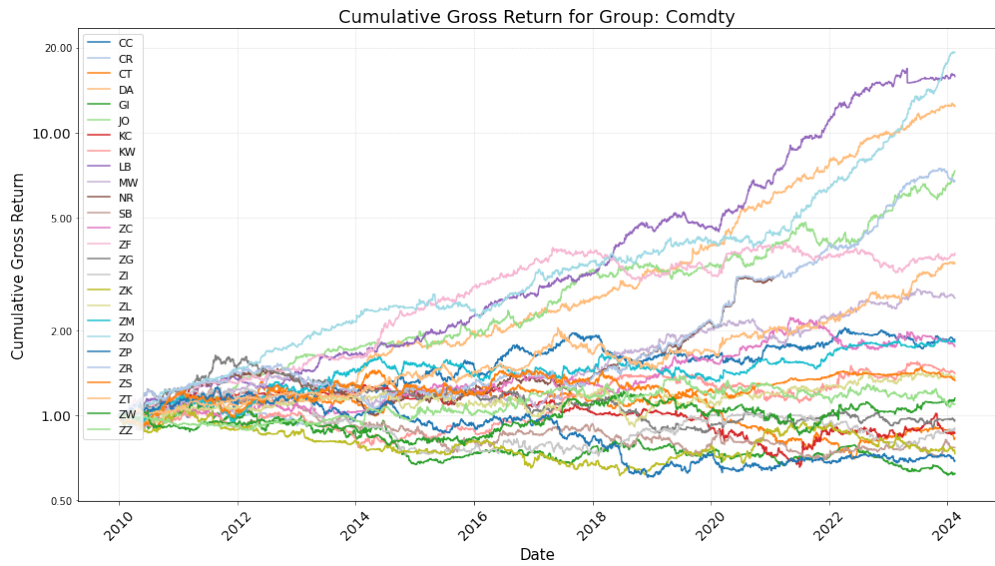


Figure 19: xLSTM PnL per asset - Commodities Futures

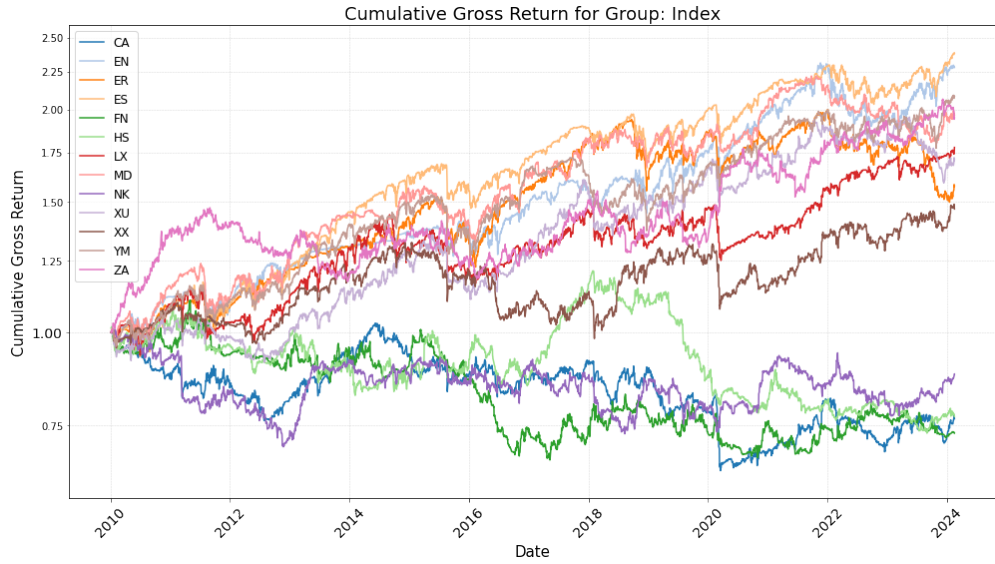


Figure 20: xLSTM PnL per asset - Index Futures

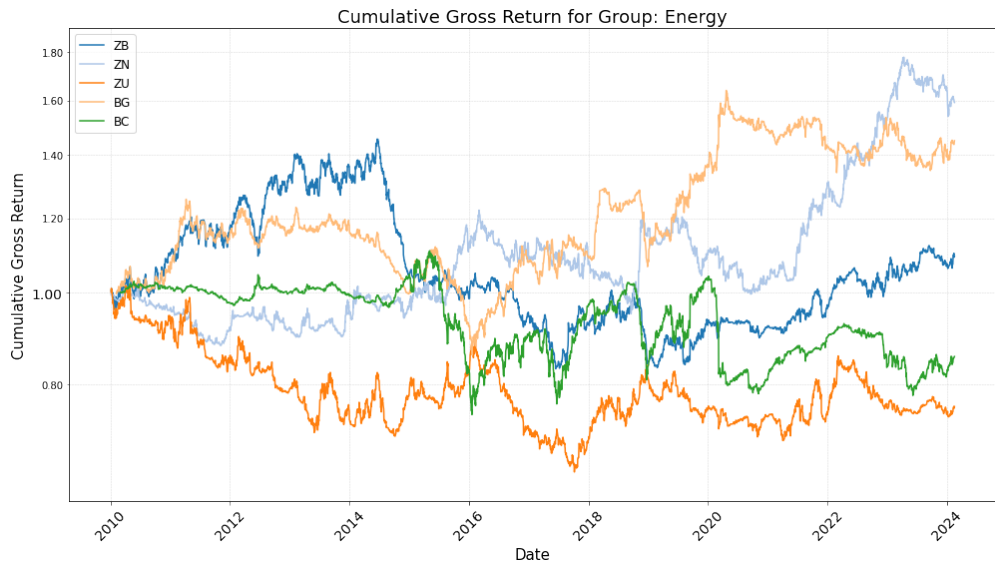


Figure 21: xLSTM PnL per asset - Energy Futures

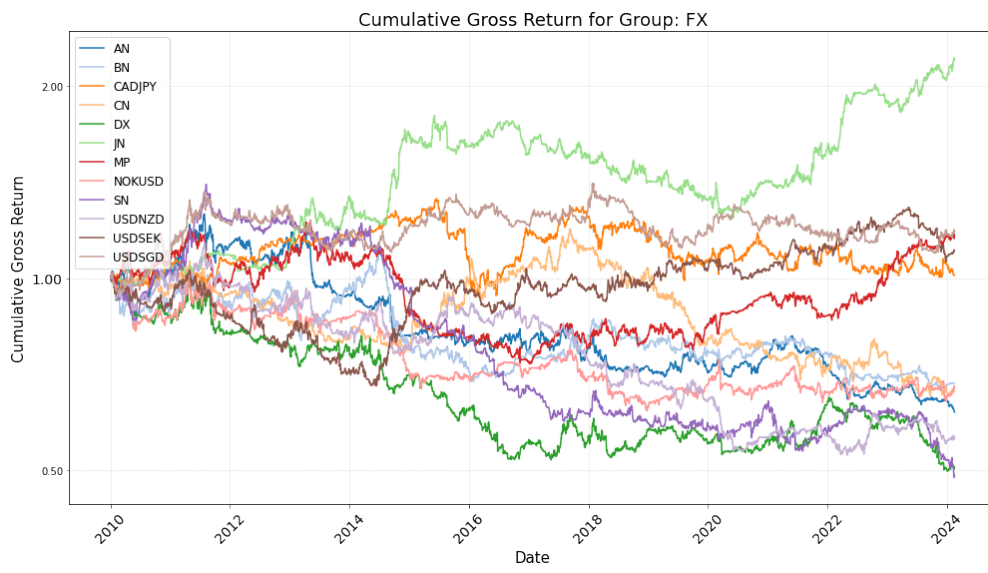


Figure 22: xLSTM PnL per asset - FX Futures

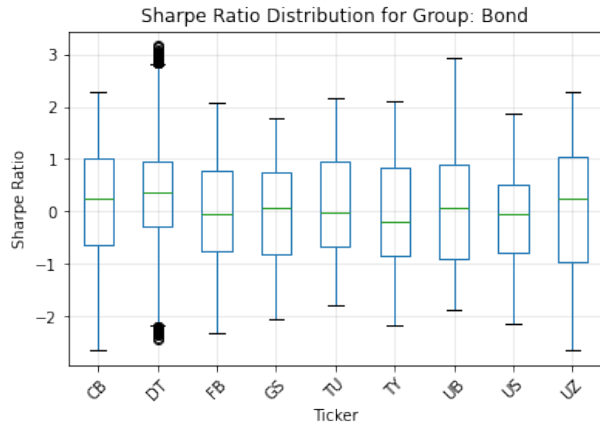


Figure 23: xLSTM box and whisker annual Sharpe Ratio per asset - Bond Futures

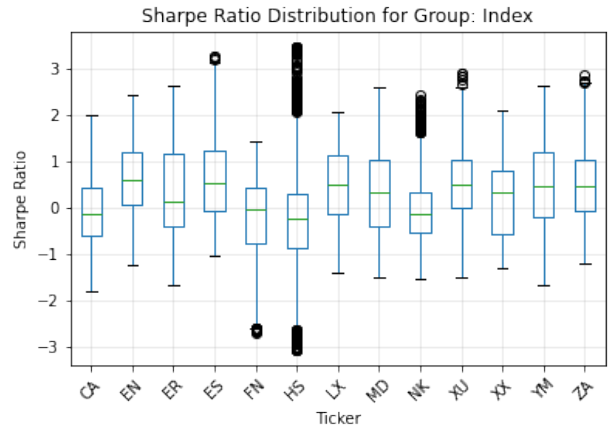


Figure 25: xLSTM box and whisker annual Sharpe Ratio per asset - Index Futures

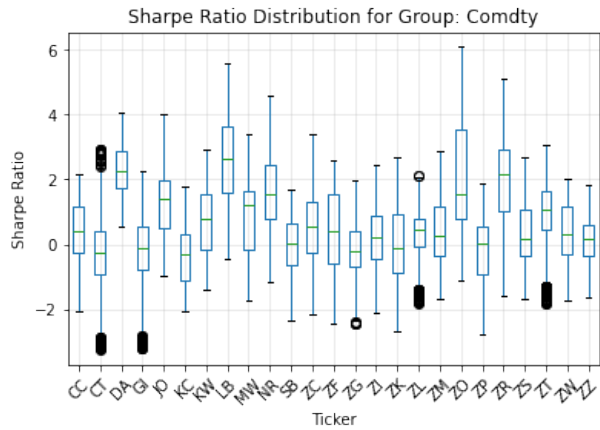


Figure 24: xLSTM box and whisker annual Sharpe Ratio per asset - Commodities Futures

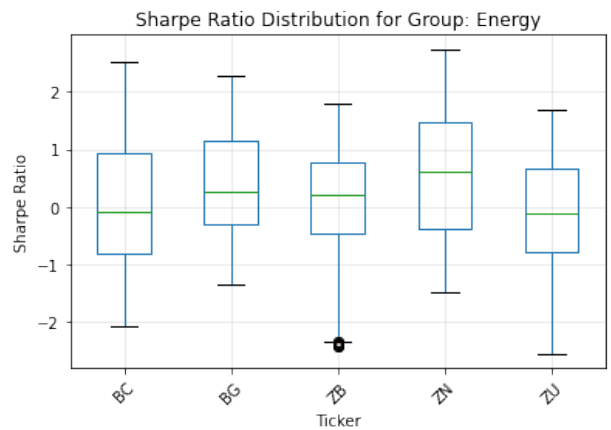


Figure 26: xLSTM box and whisker annual Sharpe Ratio per asset - Energy Futures

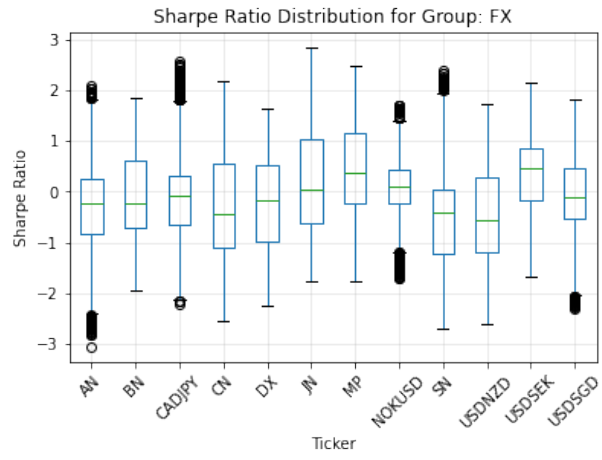


Figure 27: xLSTM box and whisker annual Sharpe Ratio per asset - FX Futures

Table 10: xLSTM: Annualised Volatility-Rescaled Performance and Breakeven Transaction Costs (bps)

Ticker	Gross (ann.)	Turnover (ann.)	$c^*$ (bps)	Ticker	Gross (ann.)	Turnover (ann.)	$c^*$ (bps)
LB	0.2338	68.93	33.92	DA	0.2200	83.29	26.41
ZO	0.2157	98.88	21.81	ES	0.0501	26.01	19.25
ZN	0.0544	29.02	18.76	CC	0.0419	24.23	17.31
EN	0.0572	38.19	14.97	JO	0.1375	96.18	14.30
ZR	0.1818	132.86	13.68	NR	0.1489	135.22	11.01
LX	0.0430	40.14	10.72	BG	0.0443	51.13	8.66
ZM	0.0279	32.54	8.57	KW	0.0587	75.50	7.77
YM	0.0409	55.80	7.33	MW	0.0824	116.51	7.07
ZT	0.0919	131.96	6.96	MP	0.0419	61.25	6.83
DT	0.0501	79.15	6.33	ZA	0.0437	76.56	5.71
ZW	0.0415	84.22	4.93	ZC	0.0471	101.33	4.65
MD	0.0325	71.83	4.53	JN	0.0336	74.70	4.50
ZZ	0.0167	42.08	3.96	ZF	0.0580	161.56	3.59
ZI	0.0211	60.24	3.50	ZS	0.0121	38.73	3.12
ER	0.0163	52.64	3.09	USDSEK	0.0286	100.11	2.85
ZL	0.0314	118.88	2.64	ZB	0.0107	41.06	2.62
XU	0.0385	151.47	2.54	UB	0.0305	176.77	1.72
XX	0.0192	178.70	1.07	CB	0.0177	217.61	0.81
GS	0.0133	223.73	0.60	NK	0.0055	145.81	0.38
ZU	0.0011	38.32	0.29	ZK	0.0032	115.80	0.28
UZ	0.0145	584.56	0.25	FB	0.0087	441.46	0.20
TU	0.0205	1121.50	0.18	TY	0.0034	219.72	0.16
USDSGD	0.0010	208.81	0.05	NOKUSD	-0.0028	102.23	-0.27
CN	-0.0106	193.52	-0.55	US	-0.0086	101.15	-0.85
CADJPY	-0.0144	166.63	-0.86	GI	-0.0072	54.74	-1.31
DX	-0.0359	270.55	-1.33	BN	-0.0143	95.74	-1.49
CA	-0.0167	110.31	-1.52	SB	-0.0084	41.65	-2.01
HS	-0.0103	45.01	-2.30	FN	-0.0193	77.30	-2.50
AN	-0.0371	131.94	-2.81	ZP	-0.0301	100.81	-2.99
ZG	-0.0190	63.04	-3.02	USDNZD	-0.0386	92.40	-4.17
CT	-0.0397	92.56	-4.29	KC	-0.0218	43.61	-4.99
SN	-0.0737	125.71	-5.86	BC	-0.0126	19.67	-6.40

**Cross-Sectional Robustness.** Taken together, the complementary results reinforce the conclusions drawn in the main text. Aggregate Sharpe ratios are not driven by isolated outliers but reflect broadly distributed performance across asset classes. Differences between models are manifested not only in overall portfolio metrics but also in dispersion characteristics and category-level stability.

This granular evaluation is particularly relevant in financial forecasting, where apparent portfolio-level improvements may otherwise mask instability or concentration risk at the instrument level.

## F Annual Sharpe Ratio

Table 11 reports annual out-of-sample Sharpe ratios for all benchmark strategies over the period 2010–2024. The year-by-year decomposition complements the aggregated results in the main text by providing

a finer assessment of temporal stability and regime dependence. Several patterns emerge. First, performance is not concentrated in a single favorable subperiod: the leading deep sequence models exhibit consistently positive Sharpe ratios across a broad range of market environments, including the post-crisis recovery, the low-volatility mid-2010s expansion, and the high-uncertainty period following 2020. Second, while cross-sectional performance rankings vary from year to year—as expected given structural shifts in volatility and cross-asset correlations—the top-performing architectures remain competitive in most years and avoid persistent underperformance. Third, classical linear benchmarks display greater sensitivity to adverse regimes, with more frequent negative annual Sharpe ratios. Overall, the annual breakdown confirms that the superior aggregated performance documented in the main text is not driven by isolated episodes, but rather reflects sustained risk-adjusted returns across heterogeneous market conditions.

Table 11: Annual Sharpe Ratios by Strategy (2010–2024)

Strategy	2010	2011	2012	2013	2014	2015	2016	2017	2018	2019	2020	2021	2022	2023	2024
AR1x	1.45	-0.07	-0.11	0.23	2.97	-0.02	0.05	0.67	-0.59	0.18	3.02	0.63	1.37	1.45	0.30
AR $n$ x	1.60	0.06	-0.25	0.06	2.51	0.22	-0.17	0.30	-0.90	0.48	2.07	0.90	1.64	1.11	-0.16
DLinear	1.21	-0.11	-0.43	-0.29	2.89	0.33	-0.19	0.42	-0.28	-0.27	3.22	0.35	1.45	2.30	-0.94
LSTM	3.58	0.29	2.47	0.74	1.81	<b>2.09</b>	2.19	-1.19	<b>1.72</b>	3.20	-1.51	1.12	3.44	1.22	1.06
VLSTM	<u>3.96</u>	<u>1.48</u>	<b>3.92</b>	<u>1.13</u>	3.03	<u>1.90</u>	<b>4.03</b>	1.06	1.33	<b>4.74</b>	0.10	2.81	<u>3.82</u>	<u>2.76</u>	-0.10
Mamba2	0.88	-0.38	-0.71	0.07	3.22	0.18	0.15	0.68	-0.05	0.00	3.15	1.33	2.27	1.43	-0.49
VSN+Mamba2	1.48	0.27	-0.12	-0.00	<b>3.43</b>	0.65	0.54	1.31	-0.05	0.23	3.31	1.92	2.64	1.45	-0.63
PatchTST	2.69	0.48	0.61	-1.21	0.72	0.24	0.13	-0.13	1.14	1.49	1.20	1.98	0.85	0.54	0.59
LPatchTST	3.90	<b>1.50</b>	3.04	0.51	<u>3.40</u>	1.60	1.72	2.39	<u>1.55</u>	3.26	1.13	<b>3.46</b>	3.24	2.57	<b>1.31</b>
PsLSTM	2.71	1.38	1.92	-0.40	2.89	1.09	1.92	1.87	1.39	2.92	1.69	<u>3.04</u>	1.74	2.29	-0.35
TFT	<b>3.97</b>	1.21	<u>3.90</u>	<b>1.19</b>	3.04	1.50	<u>3.18</u>	1.05	1.32	<u>3.36</u>	-0.14	2.62	<b>4.28</b>	<b>3.25</b>	0.37
VxLSTM	2.73	1.34	1.71	0.22	3.25	0.11	1.92	<u>2.82</u>	0.60	1.95	<u>3.77</u>	2.24	2.13	1.88	-1.31
xLSTM	2.64	1.41	1.72	-0.28	2.91	0.34	2.29	<b>2.96</b>	0.46	2.38	<b>3.83</b>	2.62	1.55	1.96	0.02
iTransformer	1.30	0.20	-1.14	0.19	2.34	0.70	-0.07	0.65	-1.16	0.21	1.43	0.95	-1.03	0.68	0.46
Mamba	0.82	-0.27	-0.46	-0.48	3.03	0.41	0.07	0.04	-0.17	-0.40	1.29	1.00	-0.54	1.47	-0.40
NLinear	1.18	0.38	-1.20	0.18	2.60	0.44	-0.22	0.96	-1.12	0.63	3.02	0.60	0.09	1.35	<u>1.07</u>